

# EXTREME IONOSPHERIC STORMS AND THEIR EFFECTS ON GPS SYSTEMS

# 23

**Geoff Crowley, Irfan Azeem**

*Atmospheric & Space Technology Research Associates (ASTRA), Boulder, CO, United States*

## CHAPTER OUTLINE

<b>1 Introduction</b> .....	555
<b>2 Global Positioning System</b> .....	557
<b>3 The Ionosphere</b> .....	558
3.1 Total Electron Content .....	559
3.2 Low-Latitude Scintillation .....	560
3.3 High-Latitude Scintillation .....	561
<b>4 Ionospheric Structures Evident in TEC Data</b> .....	565
4.1 Storm Enhanced Densities, Patches and Blobs .....	565
4.2 Traveling Ionospheric Disturbances .....	569
<b>5 Event Studies for Large Ionospheric Storms</b> .....	572
5.1 October 2003 .....	574
5.2 November 2003 .....	574
5.3 November 2004 .....	575
<b>6 System Effects of Ionospheric Storms</b> .....	575
<b>7 Discussion</b> .....	578
<b>Acknowledgments</b> .....	580
<b>References</b> .....	580
<b>Further Reading</b> .....	586

## 1 INTRODUCTION

The ionosphere is a region of the Earth's upper atmosphere from about 80 km to over 1000 km altitude that constitutes the boundary between Earth and interplanetary space. It is highly influenced by the sun and the plasma processes occurring within the Earth's magnetic field environment, as well as atmospheric waves and other disturbances propagating from the troposphere to high altitudes. The maximum

electron density in the ionosphere is normally found in the F-region between approximately 150 and 450 km. However, under some circumstances, the maximum electron density can occur in the E-region between about 100 and 150 km, either as a result of energetic particle precipitation in the auroral region, or because the F-region has decayed. Because of its plasma properties, the ionosphere interacts with a broad range of electromagnetic waves at frequencies that are important to civilian and military activities. Moreover, since the processes that influence the ionosphere vary over time scales from seconds to years, it continues to be a challenge to adequately predict its behavior in many circumstances.

Ionospheric variability is an important aspect of space weather, which refers to conditions in space (the Sun, solar wind, magnetosphere, ionosphere, or thermosphere) that can influence the performance and reliability of space-borne and ground-based technological systems. It could be argued that the most important region of variability in space weather is the ionosphere because so many applications either depend on ionospheric space weather for their operation (HF communication, over-the-horizon or OTH radar), or can be deleteriously affected by ionospheric conditions (e.g., GNSS navigation and timing, UHF satellite communications, synthetic aperture radar, HF communications, the electric power grid). As the global community becomes ever more reliant on technology, the threats from space weather increase. What is not well known is the immense degree of inter-connectedness of these technological systems, as displayed for example in Fig. 1 for Global Positioning System (GPS) applications.

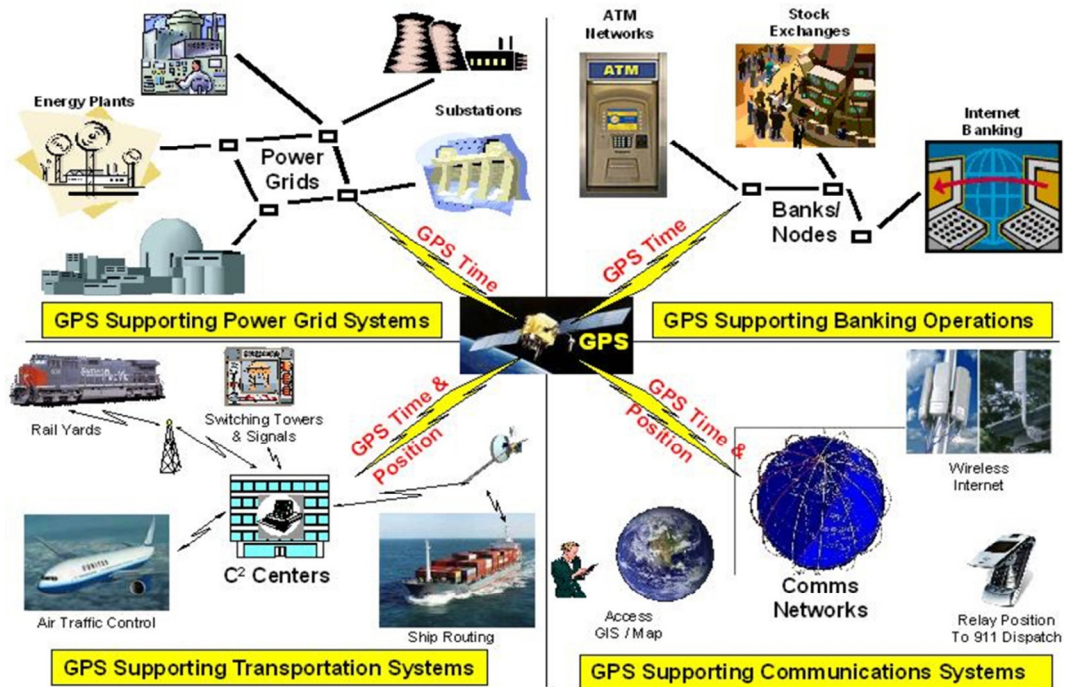


FIG. 1

Scope of interconnected critical systems dependent on availability of reliable GPS signals (after Department of Homeland Security).

The figure indicates that GPS outages can affect not only the surveyor (positioning) or farmer (precision agriculture), which are not part of the critical infrastructure, but also financial institutions, multi-modal transportation, communications systems, and the internet, and perhaps most importantly, the power grid, which relies on timing signals provided by the GPS system.

Given the importance of GPS to our modern society, this chapter examines the effects of extreme ionospheric storms on GPS/GNSS signals and systems. In [Section 2](#), we provide a brief description of the GPS satellite system and GPS signals. In [Section 3](#), we describe ionospheric storms and some of the ionospheric structures that accompany them. In [Section 4](#), we describe in more detail some of the system effects of extreme ionospheric storms – specifically on communications, navigation, and surveillance. In [Section 5](#), we describe three of the largest ionospheric storms of the last 15 years, pointing out their features captured through data analysis and modeling. We also describe the impacts of the storms on GPS signals. In [Section 6](#), we summarize some of the effects of the ionosphere on GPS systems. Finally, in [Section 7](#), we discuss the implications for extreme ionospheric storms and their effects on operational systems, with a focus on GPS-reliant systems.

---

## 2 GLOBAL POSITIONING SYSTEM

The GPS satellite constellation consists of 32 satellites (31 operational satellites) in 6 equally-spaced orbital planes at 55 degrees inclination, separated by 60 degrees right ascension of the ascending node (angle along the equator from a reference point to the orbit's intersection), and at 20,200 km altitude ([Misra and Enge, 2011](#)). Each plane contains at least four “slots” occupied by GPS satellites. This orbital geometry and the distribution of GPS satellites ensures that users on the ground can view at least four satellites from virtually any point on Earth. Each of the legacy GPS satellites broadcasts its signals continuously at two radio frequencies in the L-band of the radio spectrum. The center frequencies of these two GPS signals are at 1575.42 MHz and 1227.60 MHz, commonly referred to as L1 and L2. The original GPS signal design contained two ranging codes: the Coarse/Acquisition code or C/A, which is freely available to the public, and the Precision (encrypted) code, or P(Y)-code, reserved for DoD-authorized users. The L1 GPS signals include C/A and P(Y) codes while the L2 signal is intended for DoD users only and thus includes the P(Y) code only. On more recent satellites, a second civilian signal (L2C) and a lower L5 frequency at 1176.45 MHz have been added.

As the signals from the GPS satellites propagate through the atmosphere they undergo path delays due to the refractive index. Variation of the refractive index along the path of the signal results in bending of the propagation path making it longer than the geometrical straight-line path expected in a vacuum. This bending of the signal path, changes the apparent range between the GPS receiver and the satellite. If the refraction of the GPS signal is not accounted for, it leads to atmosphere-induced position errors. The two largest sources of errors in GPS path delays are the ionosphere and troposphere. For a typical single-frequency application, the errors introduced in GPS measurements by the ionosphere and the troposphere are on the order of 5 m and 0.5 m, respectively ([http://www.trimble.com/gps\\_tutorial/howgps-error2.aspx](http://www.trimble.com/gps_tutorial/howgps-error2.aspx)). These ionosphere errors are representative of periods when space weather is not a significant factor. It should be noted that unlike the neutral atmosphere, the ionosphere acts as a dispersive medium for RF waves, that is, the refractive index of the ionosphere is a function of frequency. As a result, refractive errors due to the ionosphere in GPS measurements can be corrected by using dual frequency GPS measurements ([Spilker, 1978](#); [Brunner and Gu, 1991](#); [Ware et al., 1996](#)).

The ionosphere can also degrade GPS receiver performance by producing diffraction of GPS signals from small-scale irregularities in the electron density distribution. These small-scale irregularities in the ionosphere, particularly those with spatial scales smaller than the Fresnel length at GPS frequencies, can produce rapid fluctuations in signal amplitude ( $C/N_0$ ) and carrier phase, called amplitude scintillation and phase scintillation, respectively. Scintillation can cause a GPS receiver to suffer from cycle slips or even loss of phase lock in conditions of severe scintillation (Doherty et al., 2000; Skone et al., 2001; Aquino et al., 2005; Sreeja et al., 2012). Severe scintillations are often observed at high (auroral) and low latitudes ( $\pm 20$  degrees of the geomagnetic equator), and in general phase scintillation is dominant at high latitudes, whereas amplitude scintillation is dominant at low latitudes, as explained in more detail in subsequent sections. Thus, it is vitally important to understand the sources and characteristics of ionospheric irregularities in order to develop predictive capabilities for scintillation events.

In addition to the GPS constellation, there are other satellite navigation systems such as GLONASS (Russia), Beidou (China), and Galileo (Europe). Like GPS, these also operate at L-band, and are therefore subject to the same ionospheric effects as GPS.

---

### 3 THE IONOSPHERE

The ionosphere is formed by the stripping away of electrons from atmospheric atoms and molecules by solar UV, EUV, and X-rays and energetic particle precipitation. Enhanced levels of X-ray and EUV light from solar flares can rapidly increase the amount of ionization and can change the height at which the ionization is created in the ionosphere. Energetic particle precipitation (typically electrons and protons) can also play a role, especially in the auroral regions. The loss of ionospheric plasma is governed by atmospheric chemistry, and by transport of plasma both downwards and out to the plasmasphere. Within the ionosphere, the plasma can be transported by both neutral winds, and by electric fields. Increased solar wind speeds and densities in some Coronal Mass Ejections (CMEs) and High Speed Streams (HSSs), along with changes in the Interplanetary Magnetic Field (IMF), can increase the high-latitude electric fields, which also increase the deposition of Joule heating and momentum into the polar neutral atmosphere. These disturbances in turn change the global thermospheric composition, temperatures, winds, and electric fields which then cause changes in the global ionosphere (e.g., Crowley et al., 1989a,b). These variations in the ionosphere can alter the propagation of radio waves in general, including GNSS radio signals. During a geomagnetic storm the interactions of the solar wind, magnetosphere, thermosphere, and ionosphere, cause dynamical changes over different spatial and temporal scales. These disturbance conditions in the ionosphere can range from large scale (100–1000 km) electron density gradients to localized (1–100 km) regions of irregular plasma structure, with embedded irregularities of less than 1 km scale size.

As noted above, the ionosphere is not uniform globally. Therefore, location will have a major impact on whether the ionosphere has a significant effect on GPS signals. We noted above that the ionospheric plasma distribution is subject to production, loss and transport processes, therefore as these processes vary with latitude, the ionospheric plasma distribution can be expected to also vary with latitude, and it is important to distinguish the ionospheric phenomena that occur at high latitudes, mid-latitudes, and low latitudes. The mid-latitude ionosphere tends to be relatively benign. In contrast, both the low-latitude and high-latitude ionosphere include significant features and structures that must be taken into account when predicting radio propagation and GPS signal variability. Furthermore, these

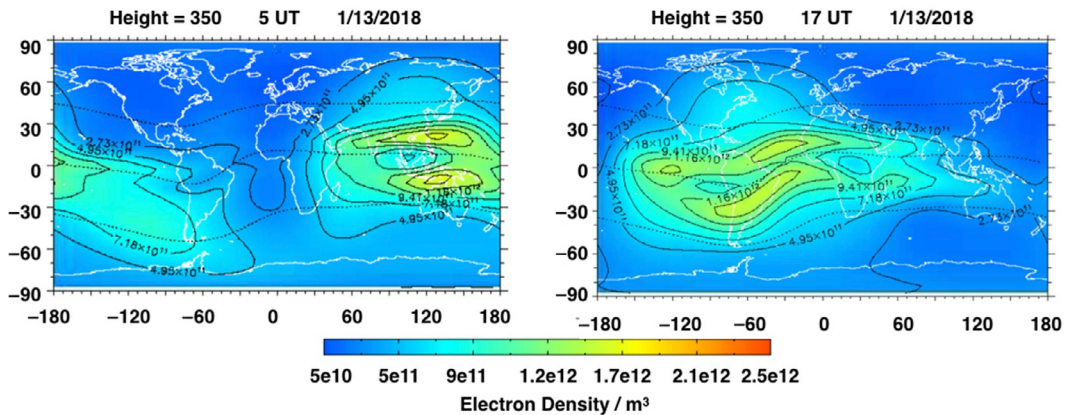


FIG. 2

Typical example of structure in the electron density at 350 km for 05 UT (*left*) and 17 UT (*right*) from the IRI climatological model predicted for January, 2018, under geomagnetically quiet conditions and low solar activity. The magnetic equator drives the location of major structures.

significant features are also very variable. Below, we describe major ionospheric features of the low-, mid-, and high-latitude ionosphere.

Fig. 2 shows the global ionospheric structure, including the Appleton Anomalies (peak values of electron density) at low latitudes, on either side of the magnetic equator. The two panels show the structure in the electron density at 350 km for 05 UT (*left*) and 17 UT (*right*) for January 2018 predicted from the IRI climatological model (Bilitza et al., 2014) under geomagnetically quiet conditions and low solar activity. These structures are also reproduced by full-physics models (e.g., Crowley et al., 2006). The Appleton Anomalies are the location of the largest electron densities and TEC. They are also the home of the most intense ionospheric irregularities, which we discuss in the next sub-section.

One way to monitor ionospheric conditions is to use specialized ground-based GPS receivers that are designed to measure ionospheric properties. These GPS receivers typically yield Total Electron Content (TEC), and some, like Atmospheric and Space Technology Research Associates (ASTRA's) CASES receivers can also measure amplitude and phase scintillation (Crowley et al., 2011; O'Hanlon et al., 2011). There are thousands of ground-based GPS receivers located across the United States and North America operated by federal, state, and local agencies, as well as private companies. Derived ionospheric data from many of these systems allow monitoring of the ionosphere, and these data could in turn be used for specification of the ionosphere-induced errors in the positioning and timing information that would be provided by the standard GNSS receivers in common use. Coster and Komjathy (2008) provided a brief history of GNSS development and its application to space weather measurements. In the sections below, we describe some of these GPS-derived TEC and scintillation measurements.

### 3.1 TOTAL ELECTRON CONTENT

The speed and propagation path of the GNSS signals in the ionosphere depend upon the number and distribution of free electrons in the path, or Total Electron Content (TEC). Changes in the TEC result in variable time delays in the signal propagation due to refraction. Space weather disturbances can cause

the ionospheric electron density profile and the corresponding TEC to vary in a variety of different ways and on different time scales. Many GNSS receivers utilize the Klobuchar ionospheric model (Klobuchar, 1987) to account for the additional delay due to ionospheric TEC. However, during intense solar and geomagnetic disturbances, the Klobuchar ionospheric model is inappropriate and can result in increased Positioning Navigation and Timing (PNT) errors particularly for single frequency GPS receivers. The PNT corrections are discussed in more detail in Section 6 of this chapter.

To support the GPS user community, various groups provide maps of TEC in real-time (e.g., Fuller-Rowell, 2005). These products often use ionospheric data assimilation models and ingest ground-based GPS data from across the United States, Canada, and Mexico to produce 2D maps of TEC. These maps can, in principle, be used to estimate the GPS signal delay due to the ionospheric TEC between a receiver and a GPS satellite. This delay can then be translated into GPS positioning error. However, this processing is non-trivial. TEC maps can be characterized in terms of RMS error and provide quantitative information about the delays. This is similar for the WAAS system, which uses a similar approach (see detailed discussion in the accompanying chapter by Mannucci and Tsurutani).

### 3.2 LOW-LATITUDE SCINTILLATION

One of the often observed impacts of ionospheric irregularities on RF communication and navigation systems is scintillation. Ionospheric scintillation is a rapid temporal fluctuation in amplitude and/or phase of a GNSS signal due to the presence of ionospheric irregularities (Kintner et al., 2007). These rapid fluctuations can be represented by computing indices called S4 and sigma-phi (Van Dierendonck, 1999). S4 and sigma-phi are computed as the normalized standard deviation of the intensity and standard deviation of the phase, respectively, over some defined time interval (typically 60 or 100 s). The refraction and diffraction effects cause group delay, phase advance, and constructive/destructive interference of the radio signal as it interacts with electron density structures in the ionosphere. Scintillations are produced when a radio wave propagating through the ionosphere undergoes diffraction due to irregularities with scale sizes less than the Fresnel length ( $L_F = (2\lambda z)^{1/2}$ , where  $\lambda$  is the wavelength and  $z$  is the distance from the irregularity to the receiver). For the GPS L1 frequency (1.5 GHz) the Fresnel length is on the order of 350 m at 350 km altitude. Scintillations, when intense, can produce message errors in satellite communication systems and may result in outages or degradation of accuracy in GNSS navigation systems. The occurrence of scintillation depends on the local time, season, solar and magnetic activity and magnetic latitude. Scintillation is most intense at low latitudes (magnetic equator and Appleton Anomalies), and at high latitudes (Aarons, 1982, 1993; Basu and Basu, 1985; Kersley et al., 1988; MacDougall, 1990; Alfonsi et al., 2011).

In the equatorial regions, ionospheric irregularities can occur on a daily basis causing severe scintillations, and especially amplitude scintillation. Here, fades at L-band can exceed 30 dB and are more severe at lower frequencies. Fig. 3 compares the carrier-to-noise ratio of scintillating and non-scintillating signals recorded simultaneously in Brazil from two GPS satellites, PRN 21 (blue curve) and PRN 25 (green curve). The received power of the scintillating PRN 21 signal varies by more than 40 dB. These fades can cause loss of GPS receiver tracking lock, increase cycle slips, lengthen acquisition times, decrease PNT accuracy, and in severe cases, cause loss of navigation if multiple satellites are affected simultaneously. For typical GPS receivers, tracking normally fails below 26 dB-Hz. At UHF frequencies, scintillations are even more severe and can interfere with satellite communication networks. Thus, GPS scintillation can serve as an index for disruptions of UHF satellite communication links.

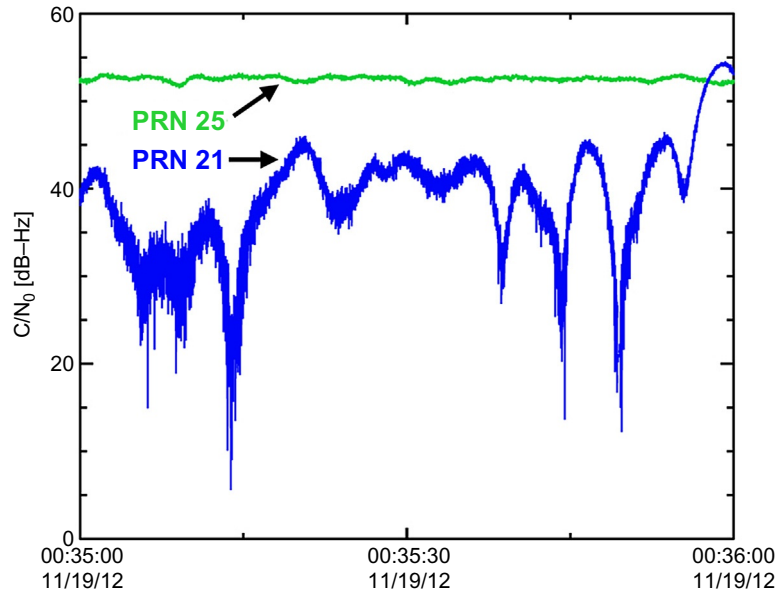


**FIG. 3**

Comparison of scintillating (PRN 21) and non-scintillating (PRN 25) signals using data taken with ASTRA CASES GPS receiver in Brazil

Low-latitude scintillation is associated with Rayleigh-Taylor instabilities that occur when the eastward electric field is enhanced and irregular plasma density depletions are generated on the bottom-side of the nighttime equatorial F region, which then rise to higher altitudes (e.g., Basu et al., 1978; Kelley, 1989; Fejer et al., 1999). The probability distribution of amplitude scintillations at low latitudes with values in excess of  $S4 = 0.5$  is highest during the post-sunset to midnight local time sector (e.g., Rama Rao et al., 2009; Steenburgh et al., 2008). Using 7 years of data, Steenburgh et al. showed that low-latitude scintillation tended to maximize at the equinoxes, and showed a strong correlation with the solar cycle.

The impact of geomagnetic storms on low-latitude amplitude scintillations remains a topic of active research. Several studies have suggested that geomagnetic storm activity will inhibit the occurrence of ionospheric irregularities and corresponding scintillations during the storm periods (Aarons, 1991; Abdu et al., 1995, and the references therein). However, studies by Basu et al. (2001a,b); and Tulasi Ram et al. (2008) have shown that in the longitude sector where the main phase of the magnetic storm happens to coincide with local sunset period, there is a greater probability that the storm-induced electric fields will enhance the post-sunset vertical drifts at the equator, resulting in conditions conducive for the onset of irregularities and ionospheric scintillations.

### 3.3 HIGH-LATITUDE SCINTILLATION

High-latitude studies generally show that phase scintillation can be severe, but that the amplitude scintillation tends to be small. There are multiple physical causes of the ionospheric irregularities that produce high-latitude scintillation, and not all are well understood. Both high-latitude particle precipitation

and convection dynamics can lead to plasma irregularities that cause scintillation of satellite signals. High-latitude GPS phase scintillation studies have shown that the variation in their occurrence rate is controlled by various factors including season and magnetic activity (Kinrade et al., 2013; Prikryl et al., 2011, 2013a,b). The main ionospheric regions that are affected by scintillation are the nightside auroral oval, the cusp/cleft on the dayside and the polar cap (Coker et al., 1995; Aarons, 1997; Aarons et al., 2000; Basu et al., 1995; Spogli et al., 2009). Using the Canadian High Arctic Ionospheric Network (CHAIN) of GPS receivers, Prikryl et al. (2010) has suggested that GPS phase scintillations are largest in the nightside auroral oval. The characteristics of the nightside phase scintillations have been shown to be significantly different from those of the dayside (cusp) ionosphere. Loucks et al. (2017) compared the climatology of phase scintillation measured in Alaska versus other sites, and pointed out the differences between auroral sites versus higher magnetic latitude polar cap sites.

To provide space weather services to GPS users and to initiate a detailed investigation of high-latitude scintillation ASTRA deployed a number of their CASES GPS receivers in Alaska, which have been operational since November 2012. These dual-frequency receivers form a longitudinal chain extending from Kaktovik to Anchorage in Alaska, and measure total electron content (TEC) and scintillation parameters, providing real-time data to users. The data and results are particularly valuable because they illustrate some of the challenges of using GPS systems for positioning and navigation in an auroral region such as Alaska.

Fig. 4 compares the GPS phase measured by a CORS receiver (*upper panel*) in Alaska, versus an ASTRA CASES receiver (*middle panel*). The CASES receivers are designed with special tracking

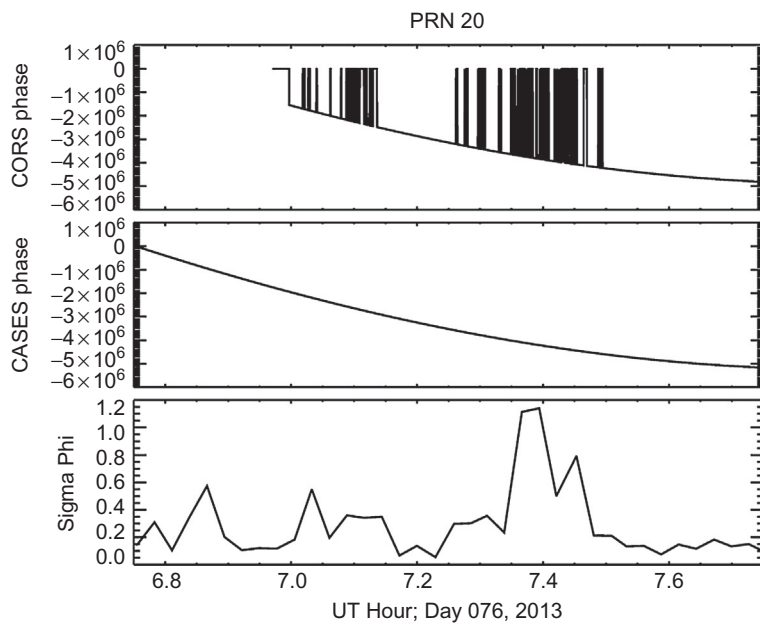


**FIG. 4**

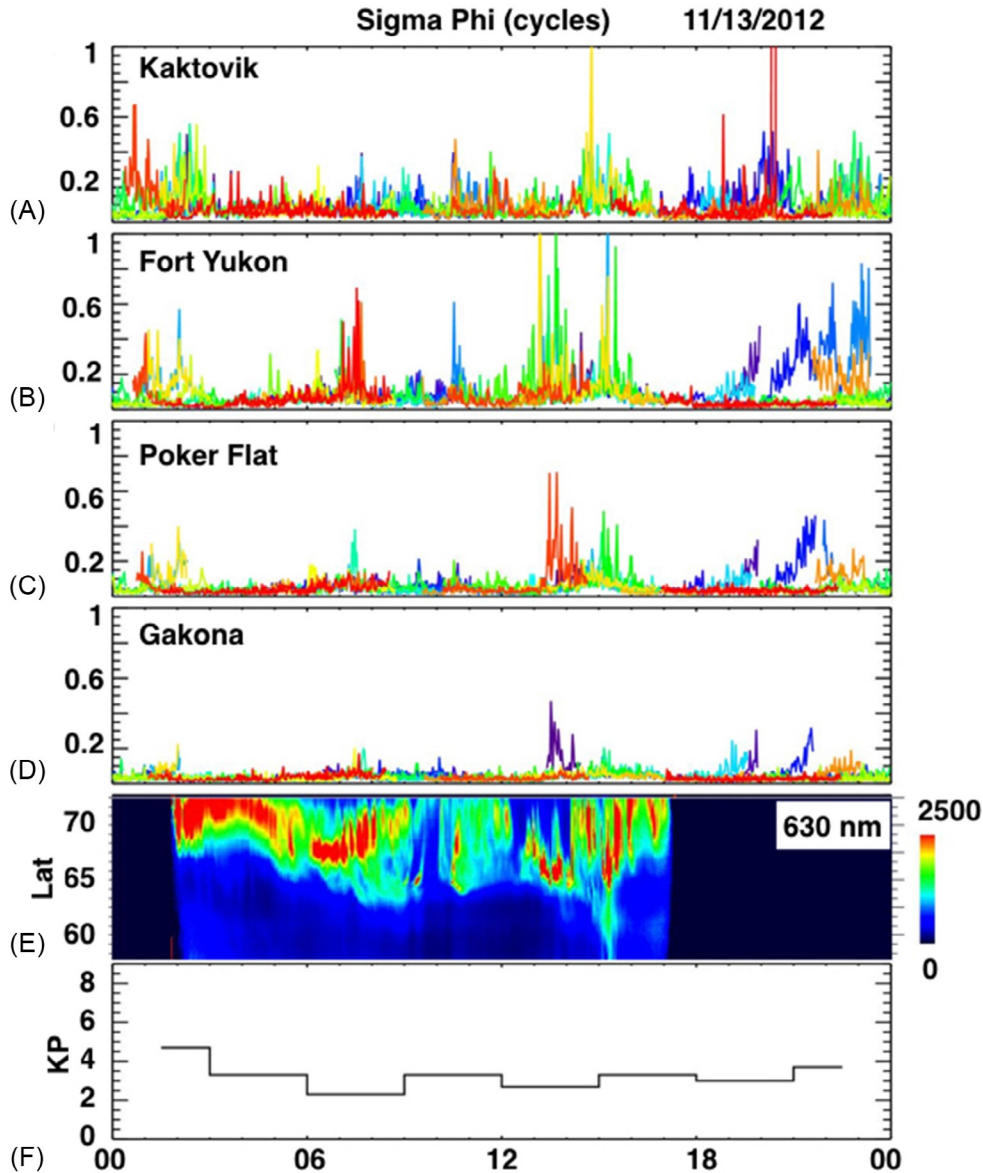
Phase measurements from CORS receiver (*upper panel*) and CASES receiver (*middle panel*) for Day 76, 2013. Lower panel shows phase scintillation index measured by CASES receiver.

loops to provide resilience against loss of lock during strong scintillation events, and the middle panel indicates a gradual phase change with no loss of lock. In contrast, the CORS receiver (*upper* panel) exhibited frequent and sustained loss of lock at this time. The lower panel illustrates the scintillation level measured by the CASES receiver, and reveals the cause of the loss of lock on the CORS receiver. Loss of lock tends to occur for the CORS receiver when the scintillation index is elevated. The CASES GPS receiver is specifically designed for monitoring and measuring ionospheric scintillations. It utilizes specialized tracking loops designed for operation in both weak-signal and scintillating environments. The incorporation of these tracking loops allows the CASES GPS receiver to provide continuous phase tracking in a scintillating environment when other GPS receivers might suffer from loss of lock.

Data from the ASTRA CASES receivers include carrier-phase and pseudo-range measurements of the L1 ( $f_1 = 1.57542$  GHz) and L2 ( $f_2 = 1.22760$  GHz) GPS signals at 1 Hz. Fig. 5 shows the variability of the phase scintillation index, sigma-phi, measured by receivers in Alaska. Fig. 5A–D shows phase scintillation activity on November 13, 2012, from four stations in the CASES Alaskan chain. The four receivers shown here are located at sites in Kaktovik (70.1 degrees N, 143.6 degrees W), Fort Yukon (66.6 degrees N, 145.2 degrees W), Poker Flat (65.1 degrees N, –147.4 degrees W), and Gakona (62.4 degrees N, –145.2 degrees W). The  $Kp$  index is plotted in the lower panel (Fig. 5F) showing that for most of the day the geomagnetic activity was low. In general, moderate phase scintillation was present on November 13, 2012. The scintillation strength during this period is largest at Kaktovik and Fort Yukon, and shows a latitudinal dependence with the southernmost receiver recording the smallest phase scintillation. In Northern Alaska, scintillation will be a frequent problem due to the omnipresence of the aurora, versus southern Alaska where it will occur predominantly near midnight.

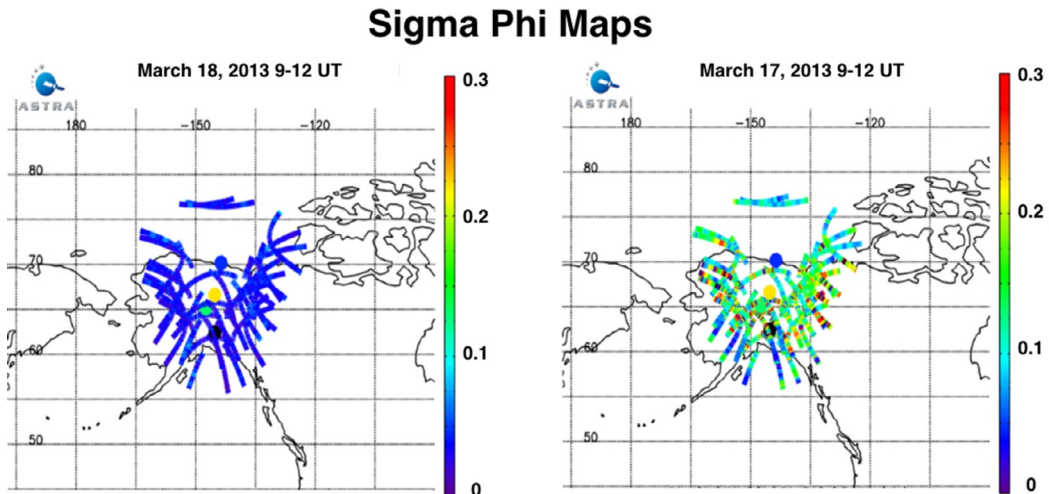
Poker Flat Research Range (PFRR) operates a meridian spectrograph to observe the location and intensity of key auroral emissions. Fig. 5 (panel-E) shows the corresponding auroral activity on November 13, 2012, measured by the PFRR meridian spectrograph. The imaging spectrograph maps a meridian slice of the sky aligned to the local magnetic meridian from horizon to horizon onto a reflection grating and collects the 2-D (spectral  $\times$  spatial) images at a 15-s cadence. Auroral emission intensities at 630.0 nm, are shown in panel-e of Fig. 5. This was geomagnetically a moderately quiet day, and most of the auroral activity was observed poleward of Poker Flat at 65 degrees N. The Meridian Spectrograph data show that auroras were generally confined to higher latitudes early in the day (2–5 UT), corresponding to the larger scintillation levels observed at the more northerly GPS sites, versus the lower latitudes. At about 6–7 UT, the auroral brightness is concentrated near 67 degrees (Fort Yukon), and there is a corresponding spike in the GPS scintillation at Fort Yukon at that time. At about 15 UT, there is a brightening of the aurora across all latitudes in Alaska, and the GPS scintillation levels at all four sites increase. We did not have meridian spectrograph data after 17 UT because of the daylight, and therefore we could not ascertain whether the later scintillation increases were correlated with auroral intensity.

ASTRA uses the CASES GPS receiver measurements to create maps of phase-scintillation in real-time ([http://cases.astraspace.net/alaska\\_sigphi.html](http://cases.astraspace.net/alaska_sigphi.html)). Fig. 6 shows the map of Alaska with phase scintillation superposed. Each panel represents 3 h of data from 9–12 UT. The arcs indicate motion of the ionospheric pierce-point during the 3 h, and the colors indicate scintillation intensity. The left panel is typical of quiet conditions, while the right panel is indicative of active conditions. We note that a relatively modest array of GPS receivers can map large regions of scintillation.

**FIG. 5**

Phase scintillation index measured by the CASES GPS receiver from (A) Kaktovik, (B) Fort Yukon, (C) Poker Flat, and (D) Gakona on November 12, 2012. (E) 630.0 nm (*red* line) auroral emissions from meridian scanning photometer; (F) 3-h Kp index. The keogram data is shown as a function of geographic latitude and UT. The emission intensity scale is in Rayleighs. Each color in the scintillation plots indicates a different PRN. Elevation mask of 20 degrees is used with GPS data to avoid spurious scintillations due to multipath effects.

*After Azeem, I., Crowley, G., Reynolds, A., Santana, J., Hampton, D., 2013. First results of phase scintillation from a longitudinal chain of ASTRA's SM-211 GPS TEC and scintillation receivers in Alaska. Proceedings of the ION 2013 Pacific PNT Meeting, April 3–25, Honolulu, Hawaii.*

**FIG. 6**

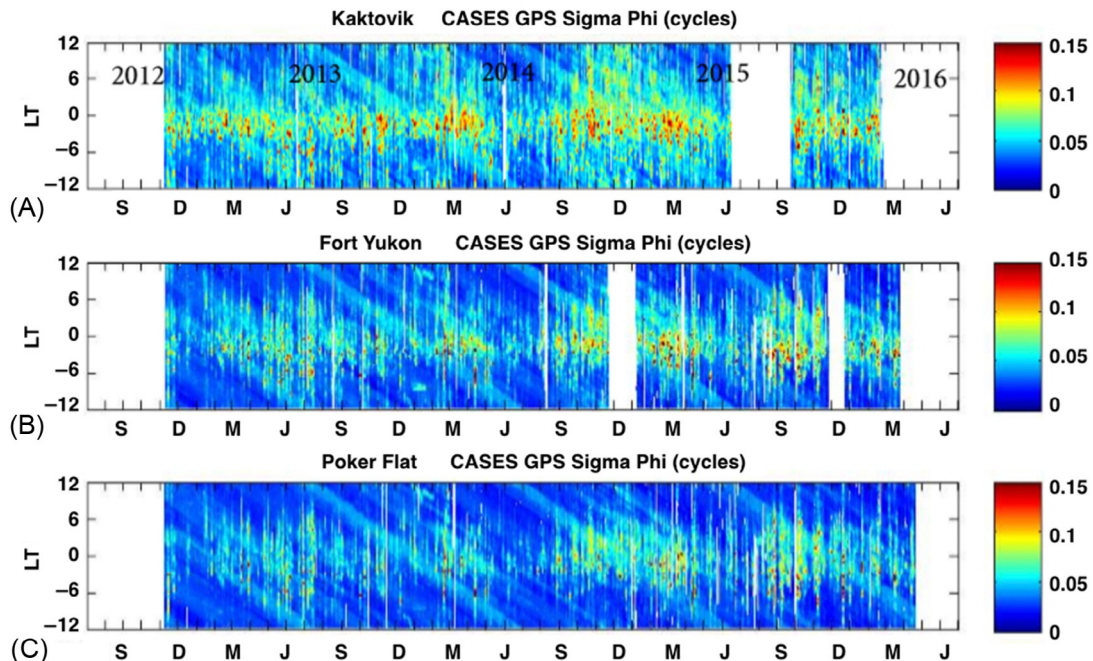
Real-time maps of ionospheric scintillation over Alaska using ASTRA's CASES GPS receivers.

Fig. 7 shows the climatology of phase scintillations measured by three of the Alaskan CASES receivers as a function of solar local time (SLT) from November 9, 2012 to February 26, 2016. The climatology is computed by binning phase scintillation data into 30-min segments for each day of observations. To minimize spurious scintillations due to multipath effects we use an elevation mask of 20 degrees to compute the climatology. The most northerly receiver site, Kaktovik, AK shows the most intense phase scintillation while Poker Flat, which is the southernmost site in the figure, on average has the smallest phase scintillation values. Phase scintillations at Kaktovik show a preponderance of large values near midnight around 1000 UT (or 2300 MLT/0100 SLT). Comparison of phase scintillation measurements from the CASES receiver stations in the Alaska GPS chain reveals two main findings: (1) Severity of phase scintillation decreases with decreasing latitude and (2) largest phase scintillations occur near magnetic midnight (Azeem et al., 2013).

## 4 IONOSPHERIC STRUCTURES EVIDENT IN TEC DATA

### 4.1 STORM ENHANCED DENSITIES, PATCHES AND BLOBS

Although the ionosphere at mid-latitudes is generally more benign than in other regions, a number of significant perturbations can occur there. In the sub-auroral region, large-scale structures like Storm Enhanced Densities (SEDs) and tongues of ionization can be present. These are enhanced plumes of electron density typically 500–1000 km in width that are transported into the polar cap where they are broken up into patches and blobs. Polar cap patches are localized enhancements in ionospheric density which originate from solar EUV ionization on the dayside, enter the polar cap at the dayside cusp, drift anti-sunward with the plasma convection at up to 1–3 km/s velocities, and then exit the polar cap near midnight to merge with sunward returning flow patterns. There is evidence that sometimes particle precipitation in the cusp or aurora may also play a role in enhancing the electron density.

**FIG. 7**

Maps of 30-min averaged phase scintillation index over nearly 4 years from 2012 to 2016, shown as a function of Local Time (LT) and day for (A) Kaktovik, (B) Fort Yukon, and (C) Poker Flat. (On the time axis, S=September, D=December, etc.)

Crowley (1996) defined polar cap patches as plasma structures with a horizontal extent of at least 100 km and a plasma density of at least twice the density of the surrounding background plasma. Crowley et al. (2000) developed a plasma trajectory analysis code that used high-latitude convection patterns and plasma drift velocities obtained from the Assimilative Mapping of Ionospheric Electrodynamics (AMIE) algorithm. They showed that long thin strands of ionospheric F-region plasma are convected from the dayside, reorganize into quasi-circular patches over the polar cap due to the differential flows in the convection pattern, and then exit the polar cap as long thin strands known as “blobs.” The trajectory code was later used with AMIE to analyze different events, and to identify and track measured patches of F-region plasma as they traversed the polar cap from the dayside to the nightside. These studies showed that the AMIE convection pattern has sufficient fidelity to specify the trajectory of plasma over the polar cap, while at the same time there is enough data for ionospheric electron density assimilation codes to specify the plasma distribution and its evolution with time.

Fig. 8 shows an example of SEDs, polar cap patches, and blobs derived from ASTRA’s ionospheric electron density assimilation code. The figure shows AMIE potential patterns plotted over the southern hemisphere plasma densities (color-scale) in geographic coordinates for four selected UTs during the SED growth and decay. Each panel is labeled with its corresponding time and the color-scale appears at the bottom right. The AMIE electric potential contours are labeled in units of kiloVolts. The outer perimeter of each map corresponds to 37 degrees S geographic latitude, and a black line with a red “X”

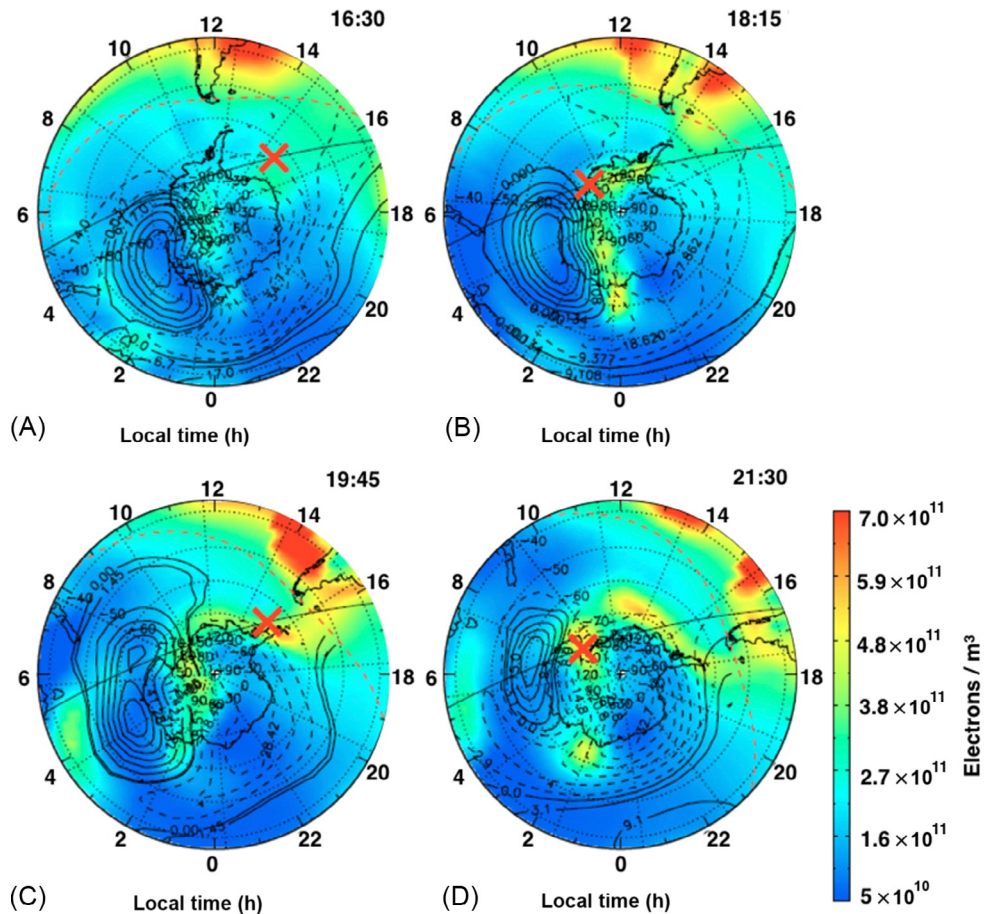


**FIG. 8**

Time evolution of the southern SED feature in electron density (color map) with AMIE potential patterns overlapped (line-contours). Results from ASTRA's assimilation algorithm are shown in geographic coordinates with the DICE orbit shown (*red* cross indicates precise DICE location at that UT). The assimilation includes data from 4559 ground-based TEC receivers, five radio occultation satellites, 3 beacon satellites combined with 32 beacon ground-stations, and 9 topside TEC instruments.

symbol indicates locations of ASTRA's DICE Cubesat (Fish et al., 2014) at this UT. By 18:15 UT (panel B) the SED plume was well developed, and a "tongue" of ionization extended from the Antarctic Peninsula near 14 LT, and between the two convection cells in the noon sector.

By this time, enhanced plasma densities appear to have been carried across the polar cap by convection, and are visible all the way into the midnight sector. A very similar structure was present at 19:45 UT (panel C), and the mid-latitude end of the SED has rotated towards a solar local time of 16 LT. By 21:30 UT the SED feature appears to originate closer to 18 LT, and wraps halfway around the dusk convection cell.

The SED in Fig. 8 occurred in the American longitude sector, and we note that SEDs do not seem to be as prevalent in other longitudes. SEDs regularly occur over the northern United States and Canada, but not in Europe, for example. Foster and Coster (2007) showed that SEDs can occur in conjugate hemispheres in the American sector. We do not understand exactly what causes SEDs, and we can only predict their occurrence and location on a statistical basis, therefore features like the SED and their effects on radio systems speak to the need for a better understanding of ionospheric variability and structure, and ultimately the need to predict its behavior more accurately.

SEDs seem to be associated with the occurrence of Sub-Auroral Plasma Streams (SAPS), which are regions of enhanced electric field. Observational data covering two solar cycles (1979–2000) from the Millstone Hill incoherent scatter radar have been used to study SAPS. The data show that there is a linear relationship between the MLT and the average magnetic latitudes (i.e., geomagnetic coordinates) in which SAPS are observed, indicating that SAPS are predominately an early evening/pre-midnight phenomenon (Foster and Vo, 2002).

Fig. 9 shows a map of North America with superposed the Foster and Vo (2002) magnetic latitude of the peak polarization stream as a function of magnetic local time (MLT) for several  $K_p$  values, from  $K_p=4$  to  $K_p=7$ .  $K_p=3$  corresponds to moderately disturbed geomagnetic conditions. The figure indicates that SAPS and therefore SEDs would not generally occur at latitudes south of Washington

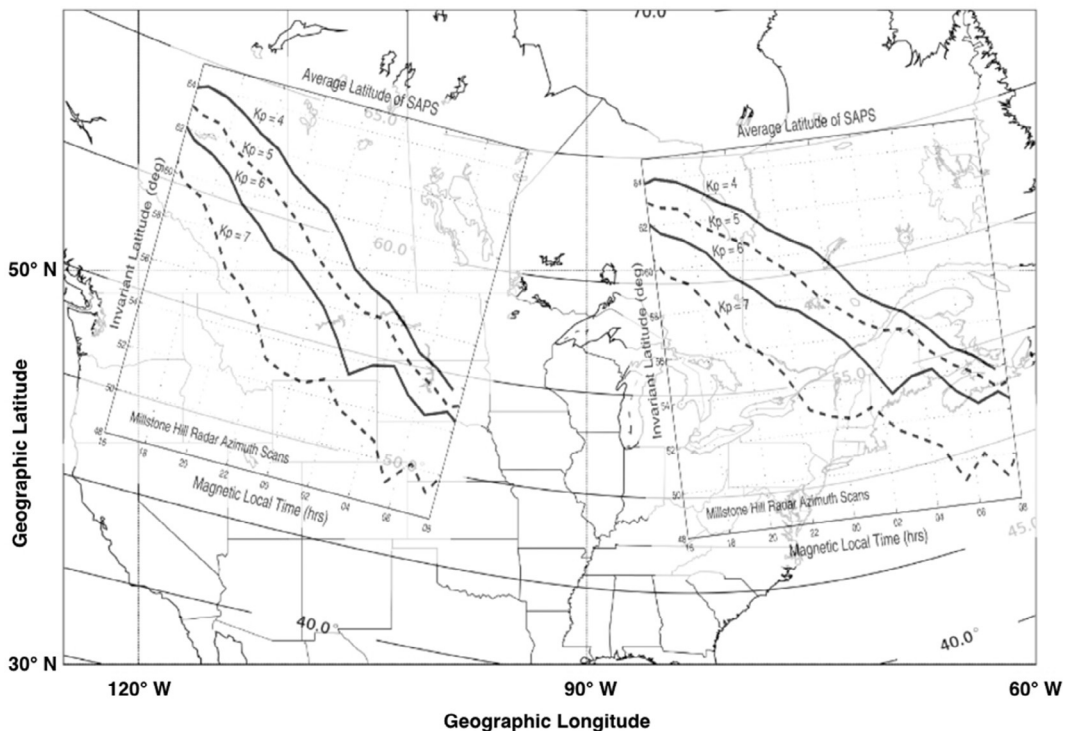


FIG. 9

Average SAPS characteristics applied to the U.S./Canadian region.

DC, although the dramatic low-latitude plasma enhancements associated with storms and SEDs occur at latitudes down to Florida and the Caribbean during Superstorm events, as indicated in Fig. 13. For completeness, we note that in the northern hemisphere Asian sector, SAPS and SEDs will occur at much higher geographic latitudes than in the United States because of the offset between the geographic and geomagnetic poles.

## 4.2 TRAVELING IONOSPHERIC DISTURBANCES

Again, although the mid-latitude ionosphere is generally considered benign, there is another type of disturbance called a Traveling Ionospheric Disturbance (TID) that can be present at almost all times and all latitudes. TIDs are propagating perturbations in the ionospheric electron density that can be detected by a number of different instruments, including ionosondes, GNSS receivers, incoherent scatter radars, and HF Doppler systems. Signatures of quasiperiodic structures detected by optical systems observing nighttime airglow emission were also linked to the occurrence of TIDs. The TID disturbance is driven by propagating acoustic gravity waves (AGWs) that perturb the ionospheric electron density. Based on their phase velocity and wave period, AGWs and classical TIDs are often classified into medium and large-scale waves. Some coarse guidelines on the properties of these two groups are summarized in Table 1. The large-scale gravity waves are generated by auroral sources. There are many sources of Medium Scale waves, including the aurora and several lower atmosphere sources including ocean waves, tsunamis, explosions, weather fronts, thunderstorms, and winds blowing over topography. Both LSTIDs and MSTIDs are thought to impact operational HF systems, and are generally considered to be the largest source of uncertainty in predicting the behavior of HF systems. Not shown in the Table are acoustic waves, below the Brunt-Vaisala period, as they are not thought to affect HF systems significantly.

TIDs and the underlying AGWs play a critical role in driving the day-to-day variability of the ionosphere. Theoretical understanding of upward AGW propagation in the atmosphere (Vadas and Crowley, 2010, 2017) suggests that while small spatial scale GWs are confined to below the stratopause, the medium and large scale AGWs have appropriate characteristic amplitudes and phase velocities to allow them to penetrate into the mesopause and ionosphere. The signature of an AGW in the ionosphere is manifested as oscillations of the ionospheric electron density resulting in a TID (Crowley and Williams, 1987; Crowley et al., 1987; Crowley and McCrea, 1988). The electron density perturbations are caused by AGWs via ion-neutral collisions (Hines, 1960; Hooke, 1968; Hocke and Schlegel, 1996).

Because of the variability of TIDs, we are unable to predict their occurrence even on a statistical basis. This variability arises from the multiple sources of gravity waves in both the troposphere and thermosphere, and the variability of the medium (background winds and temperature) through which they propagate. To add to the difficulty, both the gravity wave sources and the atmospheric medium vary with latitude, local time, and season.

**Table 1 Typical properties of medium and large-scale AGWs/TIDs**

	Period	$V_H$ (m/s)	$\lambda_H$ (km)
Medium scale	10–30 min	50–300	100–300
Large scale	0.5–5 h	300–1000	300–3000

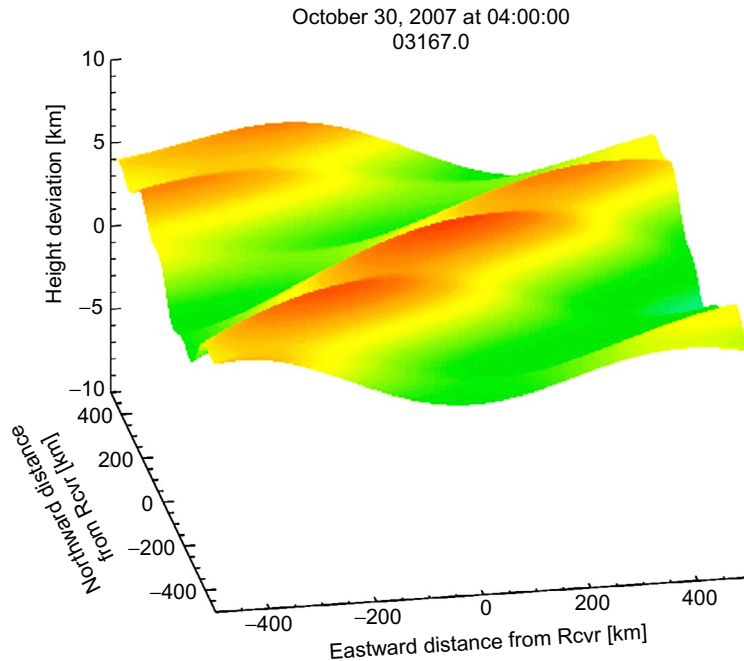


**FIG. 10**

Radio reflection surface perturbed by five TID components measured simultaneously by the TIDDBIT TID Mapping System, and extrapolated out to several hundred kilometers of horizontal distance to show the wave structure clearly. Color scale represents height perturbations from  $-10$  km to  $+10$  km. Consecutive frames can be viewed as a movie showing TIDs propagating with time.

TIDs and their effects on radio systems speak to the need for a better understanding of their morphology and climatology, and ultimately the need to predict their behavior more accurately. Before such a climatology can be constructed, more measurements of TIDs are needed, like those shown in Fig. 10 using systems like ASTRA's TIDDBIT Mapper, which provide continuous detailed TID information (Crowley and Rodrigues, 2012). The completeness of the wave information obtained from the TIDDBIT system (amplitudes, horizontal phase speeds, wavelengths, and propagation direction, vertical phase speeds all as a function of wave period) makes it possible to reconstruct the vertical displacement of radio reflection surfaces over the 200-km horizontal dimension of the sounder array. Fig. 10 illustrates a reconstruction of the TIDs/tilts for a given radio reflection surface, measured by ASTRA's TIDDBIT HF Doppler sounder array operating in Virginia, and reveals ionospheric corrugations caused by TIDs. In this figure, the wave field is comprised of five (5) wave components traveling in slightly different directions and with different speeds and wavelengths. The figure shows height perturbations of up to 10 km caused by the superposition of multiple TIDs. The resulting pattern resembles the surface of the ocean. Radio raytracing permits the effects of TIDs on operational systems to be explored. The amplitude of the TIDs depends on their source, propagation conditions, and damping factors, all of which can be difficult to determine. There is no useful F-region TID climatology at the present time that could be used to predict TID periods, amplitudes, speeds and directions at a given location.

Therefore, any operational requirement for TID information means the TID characteristics have to be measured at the required location.

While TIDDBIT provides the height perturbations of a given reflection surface, we often need to extend this to specify the ionospheric perturbations due to the TIDs at other altitudes. A number of approaches may be considered in order to extend the waves throughout the ionosphere. In practice, waves propagate with both horizontal and vertical velocity components that vary from one wave to another. Long period waves generally propagate more horizontally, while shorter period waves propagate more vertically. The TIDDBIT sounder, operating on two frequencies, can measure the vertical speed as a function of wave period. Therefore, the TIDDBIT system enables specification of both the vertical and horizontal components of wave velocity as a function of wave frequency.

Increasingly TEC measurements from networks of GPS receivers are being used to identify TIDs, and then to characterize the TID spectrum and propagation characteristics (Tsugawa et al., 2011; Nishioka et al., 2013; Crowley et al., 2016). Fig. 11 shows an example of medium scale TIDs seen in GPS TEC over the continental United States. When analyzed sequentially in time, these maps of TEC perturbations reveal that the TIDs were propagating towards the south-east for several hours. The right-hand panel in Fig. 11 shows a close-up of the TEC perturbations over Florida, where the phase-front alignment is clear.

In recent studies, ASTRA has used 5000 dual-frequency GPS receivers distributed throughout the United States to map TEC perturbations caused by TIDs (Azeem et al., 2015a,b; Crowley et al., 2016; Azeem et al., 2017), as shown in Fig. 11. Fig. 12 illustrates how the technique allows “imaging” of a wide range of TIDs including those caused by a tsunami, a thunderstorm, and auroral activity during a geomagnetic storm. Spectral analysis of these images can provide the TID frequency spectrum, horizontal phase velocities and corresponding wavelengths. We refer the reader to Azeem et al. (2017) for a detailed description of GPS TEC data processing used to create the TID maps shown in Figs. 11 and 12.

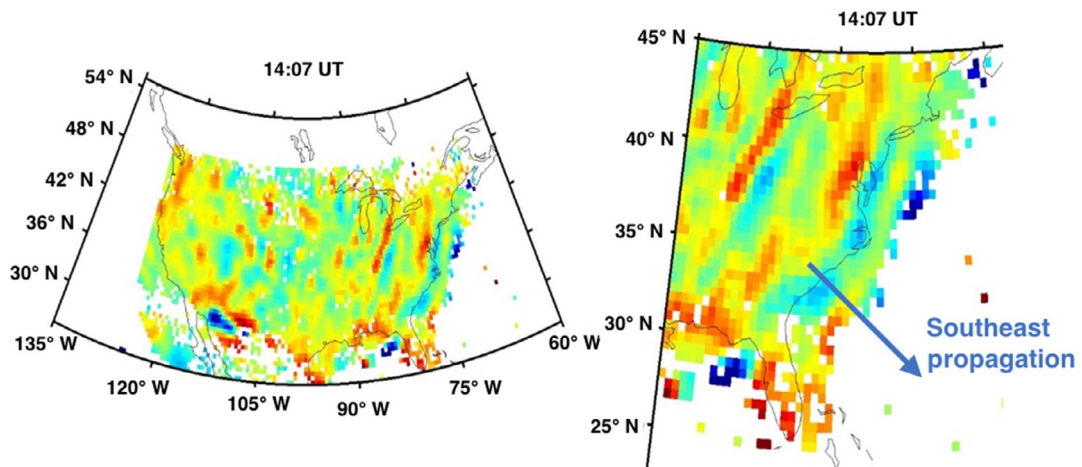


FIG. 11

Maps of GPS-TEC perturbations reveal the presence of propagating waves across the United States.

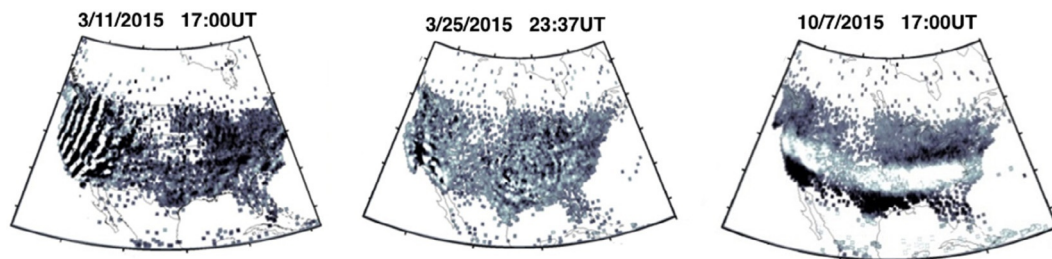


FIG. 12

GPS-TEC maps of TIDs generated by a tsunami (*left* panel), thunderstorm (*middle* panel), and auroral perturbations (*right* panel).

## 5 EVENT STUDIES FOR LARGE IONOSPHERIC STORMS

The most extreme storm on record was the Carrington event of 1859, which was described by [Tsurutani et al. \(2003\)](#). Unfortunately, there were few measurements available at the time, but newspapers reported fires in railway signals and telegraph wires due to the strong electrical currents induced in these long conductors. There was also an extreme event in 1921, and these two extreme events are described in more detail elsewhere in this book.

The Carrington event of 1859 was several times more intense than anything we have recorded in the space age ([Ngwira et al., 2013](#)). The impact of such an event today is difficult to imagine, but the most likely impact would be on the electrical grid due to the presence of long conductors. At the same time, the GPS satellites may find themselves outside of the protection of the magnetosphere, and subject to more radiation than normal, possibly causing problems with the satellite electronics. Finally, the ionospheric effects on GPS receivers could be significant. In the Carrington event, aurora sightings were reported as far south as Florida and the Caribbean, thus we would expect to see phase scintillation at most latitudes.

The largest ionospheric storms of the past 20 years occurred in October and November 2003, and in November 2004, when relatively few GPS receivers were deployed. We here describe TEC effects measured during the Halloween Storm of October 2003 to indicate the kind of effects likely to be experienced during extreme events. There have also been a number of papers published describing some of the GPS measurements obtained during these and other Super Storms, and we summarize some of those papers below.

The global thermospheric and ionospheric responses to the three superstorms mentioned above all had similarities. Specifically, the deposition of energy at high latitudes caused upwelling of the thermospheric gases, with nitrogen-rich air depleting the high-latitude ionospheric electron densities, and oxygen-rich air enhancing the low-latitude ionosphere. For the November 20, 2003, storm, these global effects were described by [Meier et al. \(2005\)](#), and by [Crowley and Meier \(2008\)](#).

Superposed on these global changes, in each superstorm were large SED events that created massively enhanced TEC values over the United States and Canada. [Fig. 13](#) depicts the TEC distribution derived from ASTRA's ionospheric electron density assimilation code for two SEDs in October 2003.

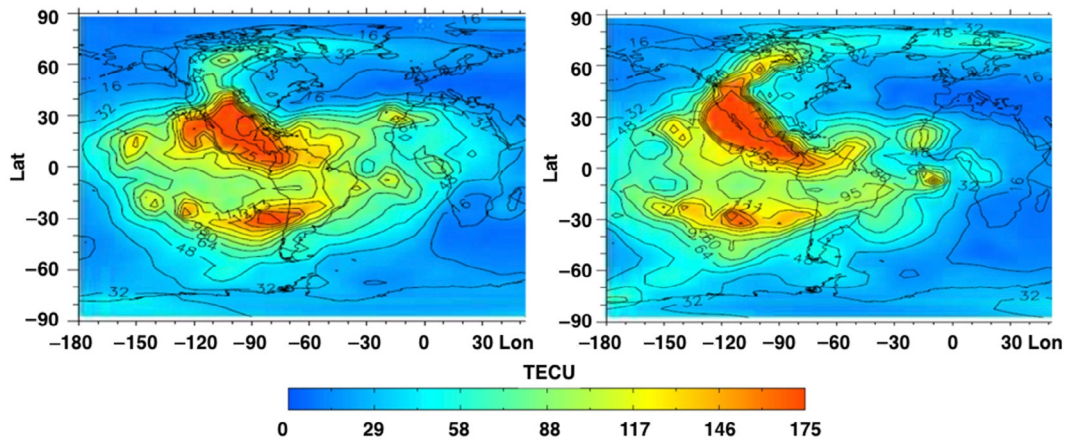


**FIG. 13**

TEC distribution for the SEDs that occurred at 21.15 UT on (*left*) Day 302, 2003, and (*right*) 21.15 UT on Day 303, 2003. These maps are generated by ASTRA's ionospheric electron density assimilation package. The assimilation includes data from 1200 ground-based TEC receivers, two radio occultation satellites, 5 beacon satellites combined with 41 beacon ground-stations, 5 topside TEC instruments, 23 ionosondes, and 3 DMSP satellites measuring in situ electron density.

These SEDs occurred on Day 302, 2003 between 20:00 to 24:00 UT (left panel), and on Day 303, 2003, between 20:00 to 24:00 UT (right panel). In each case, there is a region of enhanced mid-latitude plasma that reaches as far north as the U.S.-Canada border, and emanating from that location is a plume of plasma heading into the polar cap as a tongue of ionization that then is broken up into patches and blobs.

Fig. 14, shows the corresponding TEC values for PRN07 derived from eight (8) GPS receivers in the United States between 21:00 and 24:00 UT for each day. The receiver sites are more or less evenly spaced about 100 km apart every  $\sim 3$  degrees longitude from  $-116.3$  degrees to  $-94.7$  degrees. The GPS receivers are at latitudes of 43 degrees to 47 degrees north. In the left-hand panel, the TEC reached values of about 160 TECU, and in the right panel, TEC reached about 230 TECU. However, what is remarkable is that even though they were all observing GPS signals from the same satellite (PRN07) at any given UT, the range of TEC values observed from these eight sites differed dramatically leading to gradients of about 70 TECU per hundred kilometers which existed for several hours. Similar effects were reported by Mannucci et al. (2008) for the November 20, 2003, storm, who showed an example of severe ionospheric gradients in the mid-Atlantic region of the United States, as demonstrated by rapidly changing ranging errors (as a function of time), corresponding to about 200 TECU.

An online search reveals dozens of scientific and engineering studies that have reported on the TEC and scintillation environments of the three Superstorms considered here, as well as many other smaller storms. It is not possible to list all of them here, but the studies mentioned below can be considered representative of the types of effects that might be expected from an extreme event like the Carrington event, although we are reminded that the Carrington event was much more extreme than the three Superstorms of the past 15 years.

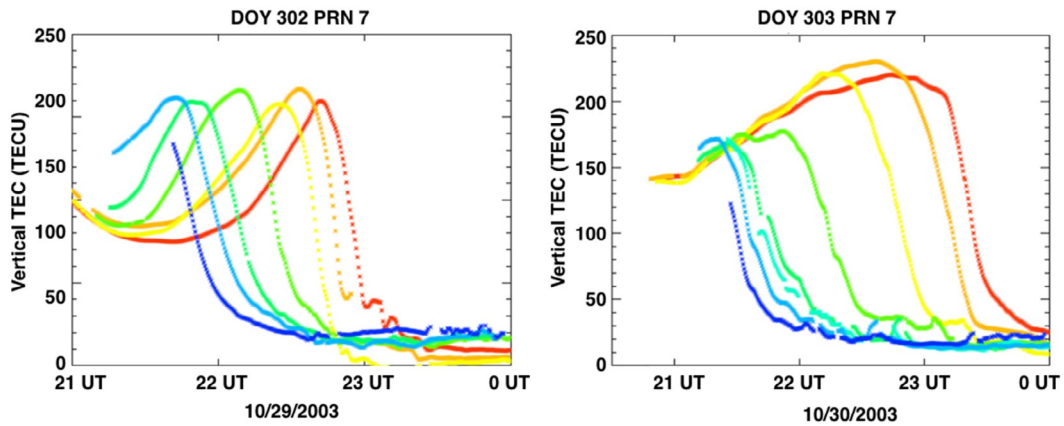


FIG. 14

TEC values from the 2003 Halloween Storm, measured from GPS receivers in the continental United States, located at longitudes of  $-116.28$ ,  $-113.24$ ,  $-111.53$ ,  $-107.00$ ,  $-103.27$ ,  $-100.82$ ,  $-97.96$ ,  $-94.72$  in a band of latitudes from 43 degrees to 47 degrees north. Only signals from PRN07 were used to construct this figure.

## 5.1 OCTOBER 2003

Mannucci et al. (2005) studied the dayside ionospheric TEC response to the storm. Mannucci et al. (2014) investigated the effect of the IMF  $B_Y$  component on the TEC response. Mannucci et al. (2008) compared the TEC response of all three superstorms listed here. Rao et al. (2010) compared the measured TEC against the TEC from the IRI model as preparation for development of the Indian SBAS system known as GPS Aided GEO Augmented Navigation (GAGAN). Bergeot et al. (2011) studied TEC variations and their impact on kinematic GPS positioning in Europe. Filjar et al. (2008) demonstrated significant vertical and horizontal positioning errors in Croatia during the storm. Mitchell et al. (2005) studied GPS TEC and scintillation measurements from the polar ionosphere. Bonelli (2008) studied scintillation in the Brazilian sector for several of the largest storms and found that scintillation is often inhibited during storms because of the westward electric field caused by the disturbance dynamo. Evans et al. (2004) described various impacts and operational challenges that occurred during the October 2003 time period.

## 5.2 NOVEMBER 2003

Meier et al. (2005), and Crowley and Meier (2008) described the development of the storm and used full physics models to explain the global changes occurring in the thermosphere and ionosphere. Kil et al. (2011) described the global TEC variations and their relationship to thermospheric composition. Astafyeva et al. (2014) described loss of lock and cycle slips from a global distribution of GPS receivers during four magnetic storms, including the November 2003 storm, and found that the loss of lock tends to peak during the maximum displacement of the geomagnetic Dst (or SYM-H) index.

### 5.3 NOVEMBER 2004

Mannucci et al. (2009) described the local time dependence of the prompt ionospheric response and TEC for the November 7, 9, and 10, 2004, superstorms. Rama Rao et al. (2009), demonstrated adverse effects on GPS, including phase slips, loss of lock, and range delay inferred from TEC in the Indian sector. Li et al. (2009) presented GPS TEC measurements of the November 2004 Superstorm in South East Asia. They found intense scintillations from low to middle latitudes in the Japanese sector during the second main phase (Nov. 10) of the storm, although the Chinese sector had no scintillation lower than 20 degrees latitude. Meggs et al. (2006) showed that the relationship between scintillation and loss of lock in northern Scandinavia depended on the receiver type.

Other large storms include the 2015 St. Patrick's Day Storm, which was the first storm of Solar Cycle 24 to reach a level of "Severe" on the NOAA geomagnetic storm scale (Wu et al., 2016). Astafyeva et al. (2015) and Carter et al. (2016) studied the global variation of plasma bubble occurrence during the storm. Jacobsen et al. (2016) provide an overview of scintillation in Norway, and its consequences for RTK and PPP positioning. Cherniak et al. (2015) and Prikryl et al. (2016) found that GPS phase scintillations were enhanced at the edge of the auroral region. Heine et al. (2017) identified small-scale irregularities along the poleward edge of the SED plume. Nayak et al. (2017) report that scintillation was suppressed in the Taiwanese sector on the storm day due to a reduced pre-reversal enhancement (PRE) in the eastward electric field, in contrast to the Indian sector, where both the PRE and scintillation were enhanced. A number of papers have described the ionospheric response in the Indian and Asian sectors (Ramsingh et al., 2015; Kakad et al., 2016; Nava et al., 2016; Tulasi Ram et al., 2016; Spogli et al., 2016). A special issue of Space Weather Journal was published in 2017 describing the responses to the St. Patrick's Day storms in 2013 and 2015 (Zhang et al., 2017, and references therein).

---

## 6 SYSTEM EFFECTS OF IONOSPHERIC STORMS

Because of its plasma properties, the ionosphere interacts with a broad range of electro-magnetic waves at frequencies that are important to civilian and military activities. Ionospheric "space weather" is one of the largest sources of error in Positioning, Navigation, and Timing (PNT) applications that use the Global Navigation Satellite System (GNSS) satellite constellations, including the U.S. government's GPS system. These space weather effects are important because GNSS signals are used by millions of people for positioning, navigation, and timing in a plethora of industries, including surveying, oil and mineral exploration, agriculture, construction, airlines, and the power industry (e.g., Hapgood, 2017).

In 2013, the U.K.'s Royal Academy of Engineering (Cannon et al., 2013) drafted a comprehensive report detailing the impacts of extreme space weather on engineered systems and infrastructure, including GNSS applications. As might be expected from the previous sections of this chapter, the main impacts will arise from TEC gradients and scintillation. Cannon et al. (2013) broke down the GPS-related infrastructure into different segments that will be impacted in different ways: single frequency receivers, dual frequency receivers, and augmented navigation systems.

- *Single-frequency* GPS receivers are now commonly used in automobile navigation systems and smart phones sold today. The single-frequency GPS receivers often operate on the L1 frequency, and their navigation accuracy is limited by ionospheric path delay. Earlier studies (Klobuchar,

1987) proposed a correction method to mitigate this delay using an empirical ionospheric model. Among the various models reported in the literature, the Klobuchar model is the one employed in most GPS receivers, and it makes use of eight broadcast coefficients (Klobuchar, 1987). As noted above, during intense solar and geomagnetic disturbances, the Klobuchar ionospheric model is inappropriate and will not be an accurate representation of the ionospheric TEC, resulting in increased PNT errors for single frequency GPS receivers. Cannon et al. point out that scintillation will add to the problem, because loss of signal from several satellites may result in greater dilution of precision, thus position errors of hundreds of meters may result, and there could even be a complete loss of positional and navigational solutions.

- *Dual-frequency* GPS receivers are an essential component of the precise position and timing services that are widely used in maritime and aviation navigation, surveying, agriculture, oil and mineral exploration, and banking industries. Dual-frequency GPS receivers require no modelling of the ionosphere because the availability of two signals, which have undergone the same ionospheric effects, is exploited to provide a direct measurement of TEC and a corresponding correction for ionospheric path delay. In the absence of measurement errors, the first-order ionospheric delay can be cancelled via a linear combination of the L1 and L2 pseudorange measurements (Misra and Enge, 2011). Thus, even in the presence of ionospheric electron density gradients, the dual-frequency receivers should remain operational. However, in an extreme event, it is likely that loss of signal from several satellites due to scintillation (e.g., Pi et al., 2017) will result in greater dilution of precision, large position errors and possibly complete loss of positional and navigational solutions. In an extreme event, Cannon et al suggest dual-frequency receivers may provide only a slight improvement over single frequency technology.
- *Augmented navigation systems* are designed to facilitate higher cadence aircraft landings by providing improved positioning and navigation capabilities. The FAA's Wide Area Augmentation System (WAAS) (Enge et al., 1996; Sparks et al., 2011a,b; ) augments the GPS system with the goal to improve accuracy, integrity and availability. It enables aircraft to rely on GPS for all phases of flight, but especially landing. WAAS consists of a network of ground-based reference receivers that measure TEC and compute a "deviation correction" (Loh et al., 1995). These measurements are routed to Master Stations, and the deviations are transmitted up to dedicated WAAS satellites in geostationary orbit every 5 s. In turn, the satellites broadcast the corrections back to Earth, where WAAS-enabled receivers onboard aircraft can utilize corrections while computing their positions to improve accuracy. The accuracy goal of WAAS is 25 ft (vertical and horizontal positioning) or better for 95% of the time. Typically, accuracies are better than 3 ft both vertically and horizontally. Various countries are deploying their own WAAS-equivalent SBAS (Satellite Based Augmentation Systems) systems, including Brazil and India.

When strong gradients in the electron density occur, as during SED events, the WAAS system recognizes the situation and notifies users not to rely on it for precision navigation until the gradients have disappeared and the situation has returned to normal. Other differential systems, including those used for precision agriculture are similarly susceptible to ionospheric gradients, although many of them will warn users of the loss of integrity.

Cannon et al. (2013) point out that during the October 2003 Halloween Superstorm, while vertical navigation guidance from WAAS was unavailable for 30 h, horizontal guidance was continuously available, and the WAAS system worked exactly as planned by increasing the error bounds at the

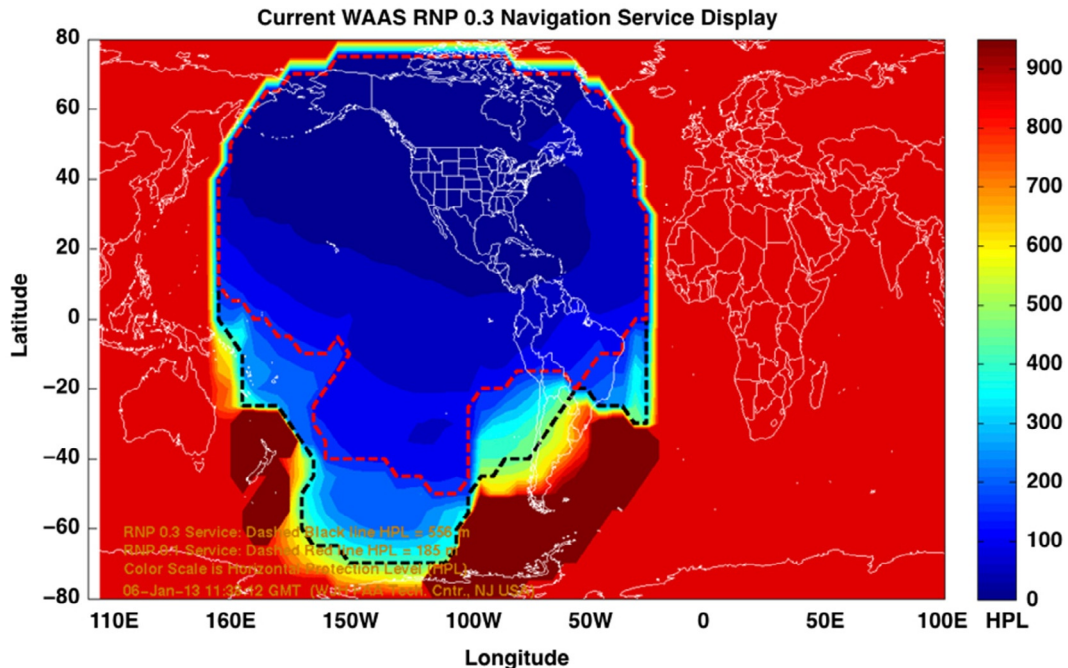


FIG. 15

Typical WAAS display showing a map of the Horizontal Protection Level (HPL). HPL is the radius of a circle in the horizontal plane (the plane tangent to the WGS-84 ellipsoid), with its center being at the true position, which describes the region that is assured to contain the indicated horizontal position. It is based upon the error estimates provided by WAAS.

affected locations. The magnitude of the October 2003 storm led to large TEC perturbations that came close to creating a hazardous situation for users, which necessitated the development of an "extreme storm detector" that has since been implemented in WAAS. This is discussed in more detail in the accompanying book chapter by Mannucci and Tsurutani (Fig. 15).

Figs. 11 and 12 depicted various TID structures seen in GPS TEC data over the Continental United States (CONUS). These TIDs in TEC data have spatial scales with a horizontal wavelength of 100 km to 3000 km, and periods of 10 min to several hours. These perturbations propagate at speeds of 50 to ~700 m/s. It is noteworthy that these TID speeds are similar to aircraft speeds, and the possibility exists that a TID and an airplane could be traveling in the same direction and at the same speed, so that the GPS receiver on the airplane "sees" a constant offset of TEC, and therefore height relative to the fixed ground systems surrounding an airport. If the TEC amplitude is large enough, the height difference between the airplane and ground-receiver could be significant enough to cause some danger. While this geometry is clear for a TID, the same problem arises for any phenomenon that causes the delay seen by the ground station to be significantly different from that seen by the airplane. Hence, SEDs and tongues of ionization that gradually move across the United States have the potential for steep TEC gradients that could similarly trigger the aforementioned situation. Clearly this is a potential problem for aircraft.

With sufficiently localized gradients, hazardous conditions could be created, as almost occurred after the storm of October 30, 2003. In the [Chapter 20](#) of the same volume, Mannucci and Tsurutani discuss a different sort of feature that arose at night, but as yet has no adequate physical explanation.

---

## 7 DISCUSSION

This paper is intended to provide an understanding of how extreme ionospheric storms can affect GPS (or GNSS) systems. The GNSS systems are primarily affected by changes in TEC, and by the ionospheric irregularities that cause scintillation. We described a number of ionospheric phenomena that can lead to changes in the TEC, and we also presented GPS TEC measurements along with scintillation measurements. The largest ionospheric storms of the past 20 years occurred in October and November 2003, and in November 2004, when few GPS receivers were deployed. Since that time, the use of GPS/GNSS has exploded. Ionospheric space weather effects are now more important than ever, because GNSS signals are used by millions of people for positioning, navigation, and timing in a plethora of industries, including surveying, oil and mineral exploration, agriculture, construction, airlines and the power industry. Most users of these applications have never experienced the impact of a significant space weather event on their systems.

During a “geomagnetic storm” or ionospheric storm, the polar cap and aurora expand to lower latitudes, and enormous amounts of energy and momentum are deposited in the high-latitude region, resulting in global changes to the ionosphere and thermosphere as described in [Section 3](#) above. The most extreme storm on record is the Carrington event of 1859, which was several times more intense than anything we have recorded in the space age ([Ngwira et al., 2013](#)). During large storms, the aurora, which is normally confined to the Arctic (or Antarctic) circle can be observed over the continental United States, United Kingdom and Europe, but in the Carrington event, auroras were reported as far south as Florida and the Caribbean. During such an event the ionospheric effects on GPS receivers would likely be significant. During large storms, the ionospheric electron densities at latitudes poleward of the aurora are significantly reduced due to upwelling molecular nitrogen gas, so the United States, Europe, Japan, and Southern Australia would experience dramatically reduced TEC compared to normal values. At other times, large variations in TEC could be expected due to dayside SEDs, polar cap patches, and nightside blobs. Because of the aurora and polar cap processes, phase scintillation could be expected throughout the United States, Europe, Japan, and Southern Australia for significant fractions of a day.

At the same time as the aurora expands equatorwards, large electric fields cause uplift of the low-latitude ionosphere, and the extent of the Appleton anomalies grows polewards. Thus, the mid-latitude ionosphere essentially disappears, squeezed by the high and low-latitude encroachment. Across Central America and Brazil, the Middle East, Southeast Asia, Northern Australia, and Africa, the Appleton anomalies will experience larger electron densities, but the embedded irregularities will generally cause scintillation within these regions.

Thus, at all latitudes, one can expect to see large changes in TEC, TEC gradients, and scintillation. At low latitudes, the amplitude scintillation will dominate, and at higher latitudes, the phase-scintillation will dominate. These changes will be modulated by variations of the Interplanetary Magnetic Field (IMF). During northward and southward IMF  $B_z$  states, penetration electric fields will diminish or enhance, respectively, the conditions that produce ionospheric irregularities and cause low-latitude scintillation. Similarly, at high latitudes, a southward IMF  $B_z$  strengthens and expands

the aurora, whereas a northward IMF (Crowley et al., 1992) can result in transpolar arcs, both conditions causing phase scintillation.

Needless to say, the effects on GPS navigation and positioning systems will likely be severe. The large TEC variability will invalidate the Klobuchar model used in single frequency systems, and scintillation will likely result in dilution of precision for positioning users. Cannon et al. (2013) note that in an extreme storm, even dual frequency systems will likely be similarly affected. SBAS systems like WAAS will experience strong TEC gradients, so they will have reduced capability that will also likely be made worse by scintillation and loss of lock.

While the use of GNSS signals to provide precise position information for navigation, tracking, and mapping is well known, their use for precise timing, time intervals, and frequency measurements is much less well known. Precise timing is crucial for a variety of economic activities around the world. Communication systems, electrical power grids, and financial networks all rely on precision timing for synchronization and operational efficiency, as noted in the introduction to this chapter. The free availability of GPS time has enabled cost savings for companies that depend on precise time and has led to significant advances in capability. Significant timing errors can cause automated systems using GPS timing data to automatically shut down. GPS-disciplined timing servers are increasingly being utilized for providing precise timing information in a diverse array of settings including power grid operations. As our nation's dependence on reliable satellite navigation systems for precise position, navigation and timing applications increases, any errors/uncertainties or degradation of service will have significant life, safety, and economic impacts. The problem is exacerbated by the fact that many new applications of GPS have been deployed in the last 5 years, during which time there were few major space weather storms because the sun was at the lowest point in its eleven-year solar cycle. Thus, there are numerous customers for GPS correction products who do not yet know they are customers. Loss of GPS timing signals may be a greater threat than positioning and navigation problems during an extreme storm.

The Halloween 2003 and November 2004 storms lasted for 3–4 days due to the solar drivers. It seems likely that an extreme storm would develop under similar circumstances and would last for several days. During that time, any systems relying on GPS (or GNSS) signals will be unreliable. For this reason, GPS-reliant systems should consider mitigation techniques to withstand GPS outages lasting several days. In both the United States and Europe, extreme space weather has been recognized as a significant threat to critical infrastructure (e.g., Evans et al., 2004; Obama, 2016), and efforts are underway to understand and mitigate against this threat.

While engineering approaches to mitigation are likely to protect critical systems during quiet times and even during Superstorms like those in 2003 and 2004, there is a danger in relying on current knowledge and experience and assuming things will be the same during an Extreme Storm like the Carrington event. There is much that is still not understood about space weather, and several examples were mentioned above. It is important to continue the current strong thrust to study and understand space weather, and especially the ionospheric phenomena that have the greatest impact on operational systems and critical infrastructure. Areas of research that should be a high priority include the complex combination of physical processes involved in SAPS and SEDs, TIDs and their climatology, scintillation and its causes. It is critical to recognize the importance of fundamental research to understand the phenomenology and physical processes involved, as well as developing engineering solutions to mitigate the effects of space weather. Without understanding the physics and the phenomena, it seems likely that mitigation solutions will address perceived problems, but may lack the fundamental underpinning to avoid other phenomena that may be less common and just as dangerous or destructive.

---

## ACKNOWLEDGMENTS

We are grateful for the opportunity to describe and explain ionospheric space weather and its potential impact on GPS systems and GPS-reliant technologies. We dedicate this chapter to the memory of our friend Dr. Paul Kintner of Cornell University who did so much to promote measurements of scintillation. His invention of the “Scintmon” receiver and his partnership with ASTRA led to the development and commercialization of the CASES receiver and later generations of ASTRA’s scintillation monitors. GC’s work at ASTRA was supported by Air Force contract FA9453-13-C-0035, ONR grant N00014-13-1-0343, NSF grants AGS-1144062 and AGS-1623962, and NASA grant NNX14AP88G. IA’s participation in this study was supported by NASA contract NNH13CJ33C and NSF grant AGS-1552310 to ASTRA.

---

## REFERENCES

- Aarons, J., 1982. Global morphology of ionospheric scintillations. *Proc. IEEE* 70 (4), 360–378.
- Aarons, J., 1991. The role of the ring current in the generation or inhibition of equatorial F layer irregularities during magnetic storms. *Radio Sci.* 26 (04), 1131–1149.
- Aarons, J., 1993. The longitudinal morphology of equatorial F-layer irregularities relevant to their occurrence. *Space Sci. Rev.* 63 (3), 209–243.
- Aarons, J., 1997. Global positioning system phase fluctuations at auroral latitudes. *J. Geophys. Res.* 102, 17219–17231. <https://doi.org/10.1029/97JA01118>.
- Aarons, J., Lin, B., Mendillo, M., Liou, K., Codrescu, M., 2000. Global Positioning System phase fluctuations and ultraviolet images from the Polar satellite. *J. Geophys. Res.* 105, 5201–5213. <https://doi.org/10.1029/1999JA900409>.
- Abdu, M.A., Batista, I.S., Walker, G.O., Sobral, J.H.A., Trivedi, N.B., De Paula, E.R., 1995. Equatorial ionospheric electric fields during magnetospheric disturbances: local time/longitude dependences from recent EITS campaigns. *J. Atmos. Terres. Phys.* 57 (10), 1065–1083.
- Alfonsi, L., Spogli, L., De Franceschi, G., Romano, V., Aquino, M., Dodson, A., Mitchell, C.N., 2011. Bipolar climatology of GPS ionospheric scintillation at solar minimum. *Radio Sci.* 46, RS0D05. <https://doi.org/10.1029/2010RS004571>.
- Aquino, M., Moore, T., Dodson, A., Waugh, S., Souter, J., Rodrigues, F.S., 2005. Implications of ionospheric scintillation for GNSS users in northern Europe. *J. Navig.* 58, 241–256. <https://doi.org/10.1017/S0373463305003218>.
- Astafyeva, E., Yasyukevich, Y., Maksikov, A., Zhivetiev, I., 2014. Geomagnetic storms, super-storms, and their impacts on GPS-based navigation systems. *Space Weather* 12, 508–525. <https://doi.org/10.1002/2014SW001072>.
- Astafyeva, E., Zakharenkova, I., Förster, M., 2015. Ionospheric response to the 2015 St. Patrick’s Day storm: a global multi-instrumental overview. *J. Geophys. Res.* 120 (2015), 9023–9037. <https://doi.org/10.1002/2015JA02162>.
- Azeem, I., Crowley, G., Reynolds, A., Santana, J., Hampton, D., 2013. First results of phase scintillation from a longitudinal chain of ASTRA’s SM-211 GPS TEC and Scintillation Receivers in Alaska. In: *Proceedings of the ION 2013 Pacific PNT Meeting, April 23–25, Honolulu, Hawaii*, .
- Azeem, I., Crowley, G., Honniball, C., 2015a. Global ionospheric response to the 2009 sudden stratospheric warming event using Ionospheric Data Assimilation Four-Dimensional (IDA4D) algorithm. *J. Geophys. Res. Space Phys.* 120. <https://doi.org/10.1002/2015JA020993>.
- Azeem, I., Yue, J., Hoffmann, L., Miller, S.D., Straka III, W.C., Crowley, G., 2015b. Multisensor profiling of a concentric gravity wave event propagating from the troposphere to the ionosphere. *Geophys. Res. Lett.* 42. <https://doi.org/10.1002/2015GL065903>.

- Azeem, I., Vadas, S.L., Crowley, G., Makela, J.J., 2017. Traveling ionospheric disturbances over the United States induced by gravity waves from the 2011 Tohoku tsunami and comparison with gravity wave dissipative theory. *J. Geophys. Res.* 122. <https://doi.org/10.1002/2016JA023659>.
- Basu, Su., Basu, S., 1985. Equatorial scintillations: advances since ISEA-6. *J. Atmos. Terres. Phys.* 47, 753–768. [https://doi.org/10.1016/0021-9169\(85\) 90052-2](https://doi.org/10.1016/0021-9169(85) 90052-2).
- Basu, S., Basu, S., Aarons, J., McClure, J., Cousins, M., 1978. On the coexistence of kilometer- and meter-scale irregularities in the Nighttime Equatorial F region. *J. Geophys. Res.* 83 (A9), 4219–4226.
- Basu, S., Basu, S., Sojka, J.J., Schunk, R.W., MacKenzie, E., 1995. Macroscale modeling and mesoscale observations of plasma density structures in the polar cap. *Geophys. Res. Lett.* 22, 881–884. <https://doi.org/10.1029/95GL00467>.
- Basu, S., et al., 2001a. Ionospheric effects of major magnetic storms during the international space weather period of September and October 1999: GPS observations, VHF/UHF scintillations, and in situ density structures at middle and equatorial latitudes. *J. Geophys. Res.* 106 (A), 30389–30414. <https://doi.org/10.1029/2001JA001116>.
- Basu, S., Basu, S., Groves, K.M., Yeh, H.C., Su, S.Y., Rich, F.J., Sultan, P.J., Keskinen, M.J., 2001b. Response of the equatorial ionosphere in the South Atlantic Region to the Great Magnetic Storm of July 15, 2000. *Geophys. Res. Lett.* 28 (18), 3577–3580. <https://doi.org/10.1029/2001GL013259>.
- Bergeot, N., Bruyninx, C., Defraigne, P., Pireaux, S., Legrand, J., Pottiaux, E., Baire, Q., 2011. Impact of the Halloween 2003 ionospheric storm on kinematic GPS positioning in Europe. *GPS Solutions* 15, 171–180.
- Bilitza, D., Altadill, D., Zhang, Y., Mertens, C., Truhlik, V., Richards, P., McKinnell, L.-A., Reinisch, B., 2014. The International Reference Ionosphere 2012-A model of international collaboration. *J. Space Weather Space Clim.* 4, A07–A13. <https://doi.org/10.1051/swsc/2014004>.
- Bonelli, E., 2008. Attenuation of GPS scintillation in Brazil due to magnetic storms. *Space Weather.* 6(9).
- Brunner, F., Gu, M., 1991. An improved model for the dual frequency ionospheric correction of GPS observations. *Manuscr Geodaet* 16, 205–214.
- Cannon, P.S., et al., 2013. Extreme Space Weather: Impacts on Engineered Systems. Royal Academy of Engineering, London, UK. p. 68. Available at <http://www.raeng.org.uk/publications/reports/space-weather-full-report>.
- Carter, B.A., Yizengaw, E., Pradipta, R., Retterer, J.M., Groves, K., Valladares, C., Caton, R., Bridgwood, C., Norman, R., Zhang, K., 2016. Global equatorial plasma bubble occurrence during the 2015 St. Patrick's Day storm. *J. Geophys. Res.* 121 (2016), 894–905. <https://doi.org/10.1002/2015JA02219>.
- Cherniak, L., Zakharenkova, I., Redmon, R.J., 2015. Dynamics of the high-latitude ionospheric irregularities during the 17 March 2015 St. Patrick's Day storm: ground-based GPS measurements. *Space Weather* 13 (2015), 585–597. <https://doi.org/10.1002/2015SW00123>.
- Coker, C., Hunsucker, R., Lott, G., 1995. Detection of auroral activity using GPS satellites. *Geophys. Res. Lett.* 22 (23), 3259–3262. <https://doi.org/10.1029/95GL03091>.
- Coster, A., Komjathy, A., 2008. Space weather and the Global Positioning System. *Space Weather* 6, S06D04. <https://doi.org/10.1029/2008SW000400>.
- Crowley, G., 1996. Critical review on ionospheric patches and blobs. In: *The Review of Radio Science 1992–1996*. Oxford University Press.
- Crowley, G., McCrear, I.W., 1988. A synoptic study of TIDs observed in the UK during the first WAGS campaign, October 10-18, 1985. *Radio Sci.* 23, 905–917.
- Crowley, G., Meier, R.R., 2008. Disturbed O/N<sub>2</sub> ratios and their transport to middle and low latitudes, AGU Mid-latitude Ionospheric Dynamics and Disturbances. *AGU Geophys. Monograph Ser.* 181, 221–234.
- Crowley, G., Rodrigues, F., 2012. Characteristics of traveling ionospheric disturbances observed by the TIDDBIT Sounder. *Radio Sci.* 47, RS0L22. <https://doi.org/10.1029/2011RS004959>.
- Crowley, G., Williams, P.J.S., 1987. Observation of the source and propagation of atmospheric gravity waves. *Nature* 328, 231–233.
- Crowley, G., Jones, T.B., Dudeney, J.R., 1987. Comparison of short period TID morphologies in Antarctica during geomagnetically quiet and active intervals. *J. Atmos. Terres. Phys.* 49, 155.

- Crowley, G., Emery, B.A., Roble, R.G., Carlson, H.C., Knipp, D.J., 1989a. Thermospheric dynamics during Sept. 18 and 19, 1984, Model Simulations. *J. Geophys. Res.* 94, 16925–16944.
- Crowley, G., Emery, B.A., Roble, R.G., Carlson, H.C., Salah, J.E., Wickwar, V.B., Miller, K.L., Oliver, W.L., Burnside, R.G., Marcos, F.A., 1989b. Thermospheric dynamics during the Equinox Transition study of September 1984 II. Validation of the NCAR-TGCM. *J. Geophys. Res.* 94, 16945–16960.
- Crowley, G., Cannon, P.S., Dozois, C.G., Reinisch, B.W., Buchau, J., 1992. Polar cap convection for  $B_z$  northward. *Geophys. Res. Lett.* 19, 657–660.
- Crowley, G., Ridley, A.J., Deist, D., Wing, S., Knipp, D.J., Emery, B.A., Foster, J., Heelis, R., Hairston, M., Reinisch, B.W., 2000. The transformation of high-latitude ionospheric F-region patches into blobs during the March 21, 1990 storm. *J. Geophys. Res.* 105, 5215–5230.
- Crowley, G., Hackert, C., Meier, R.R., Strickland, D.J., Paxton, L.J., Pi, X., Manucci, A., Christensen, A., Morrison, D., Bust, G., Roble, R.G., Curtis, N., Wene, G., 2006. Global thermosphere-ionosphere response to onset of November 20, 2003 Magnetic Storm. *J. Geophys. Res.* 111, A10S18. <https://doi.org/10.1029/2005JA011518>.
- Crowley, G., Bust, G.S., Reynolds, A., Azeem, I., Wilder, R., O’Hanlon, B.W., Psiaki, M.L., Powell, S., Humphreys, T.E., Bhatti, J.A., 2011. CASES: a novel low-cost ground-based dual-frequency GPS software receiver and space weather monitor. In: Proceedings of the 24th International Technical Meeting of The Satellite Division of the Institute of Navigation, Portland, OR, pp. 1437–1446.
- Crowley, G., Azeem, I., Reynolds, A., Duly, T.M., McBride, P., Winkler, C., Hunton, D., 2016. Analysis of traveling ionospheric disturbances (TIDs) in GPS TEC launched by the 2011 Tohoku earthquake. *Radio Sci.* 51, 507–514. <https://doi.org/10.1002/2015RS005907>.
- Doherty, P.H., Delay, S.H., Valladares, C.E., Klobuchar, J.A., 2000. Ionospheric Scintillation Effects in the Equatorial and Auroral Regions. Paper presented at GPS 2000, Institute of Navigation, Salt Lake City, Utah.
- Enge, P., Walter, T., Pullen, S., Kee, C., Chao, Y.-C., Tsai, Y.-J., 1996. Wide area augmentation of the global positioning system. *Proc. IEEE* 84, 1063–1088.
- Evans, D.L., Lautenbacher, C.C., Rosen, R.D., Johnson, D.L., 2004. Intense Space Weather Storms October 19–Nov 7, 2003, Service assessment, U.S. Dept of Commerce, National Weather service, Silver Spring, Maryland.
- Fejer, B.G., Scherliess, L., de Paula, E.R., 1999. Effects of the vertical plasma drift velocity on the generation and evolution of equatorial spread F. *J. Geophys. Res.* 104, 19859–19869.
- Filjar, R., Kos, T., Cicin, V., 2008. GPS positioning performance in the wake of the Halloween 2003 geomagnetic storm. Published in proceedings of IEEE ELMAR 50th International Symposium, Zadar, Croatia, ISSN: 1334-2630.
- Fish, C.S., Swenson, C.M., Crowley, G., Barjatya, A., Neilsen, T., Gunther, J., Azeem, I., Pilinski, M., Wilder, R., Cook, J., Nelsen, J., Burt, R., Whiteley, M., Bingham, B., Hansen, G., Wassom, S., Davis, K., Jensen, S., Patterson, P., Young, Q., Petersen, J., Schaire, S., Davis, C.R., Bokaie, M., Fullmer, R., Baktur, R., Sojka, J., Cousins, M., 2014. Design, development, implementation, and on orbit performance of the dynamic ionosphere CubeSat experiment mission. *Space Sci. Rev.* 181, 61–120. <https://doi.org/10.1007/s11214-014-0034-x>.
- Foster, J.C., Coster, A.J., 2007. Conjugate localized enhancement of total electron content at low latitudes in the American sector. *J. Atmos. Sol. Terr. Phys.* 69, 1241–1252.
- Foster, J.C., Vo, H.B., 2002. Average characteristics and activity dependence of the subauroral polarization stream. *J. Geophys. Res.: Space Phys.* 107(A12).
- Fuller-Rowell, T., 2005. USTEC: a new product from the Space Environment Center characterizing the ionospheric total electron content. *GPS Solutions* 9 (3), 236–239.
- Hapgood, M., 2017. Satellite navigation—amazing technology but insidious risk: why everyone needs to understand Space Weather. *Space Weather* 15, 545–548. <https://doi.org/10.1002/2017SW001638>.
- Heine, T.R.P., Moldwin, M.B., Zou, S., 2017. Small-scale structure of the mid-latitude storm enhanced density plume during the March 17, 2015 St. Patrick’s Day storm. *J. Geophys. Res.* 122, 3665–3677. <https://doi.org/10.1002/2016JA022965>.

- Hines, C.O., 1960. Internal atmospheric gravity waves at ionospheric heights. *Can. J. Phys.* 38, 1441–1481.
- Hocke, K., Schlegel, K., 1996. A review of atmospheric gravity waves and travelling ionospheric disturbances: 1982–1995. *Ann. Geophys.* 14 (9), 917.
- Hooke, W.H., 1968. The response of the F-region ionosphere to internal atmospheric gravity waves. In: *Acoustic-Gravity Waves in the Atmosphere*. p. 367.
- Jacobsen, K.S., et al., 2016. Overview of the 2015 St. Patrick's Day storm and its consequences for RTK and PPP positioning in Norway. *J. Space Weather Space Climate* 6, 12. <https://doi.org/10.1051/swsc/2016004.id.A9>.
- Kakad, B., Gurram, P., Tripura Sundari, P.N.B., Bhattacharyya, A., 2016. Structuring of intermediate scale equatorial spread F irregularities during intense geomagnetic storm of solar cycle 24. *J. Geophys. Res.* 121 (2016), 7001–7012. <https://doi.org/10.1002/2016JA022635>.
- Kelley, M.C., 1989. *The Earth's Ionosphere, Plasma Physics and Electrodynamics*. Academic, San Diego.
- Kersley, L., Pryse, S.E., Wheadon, N.S., 1988. Amplitude and phase scintillation at high latitudes over northern Europe. *Radio Sci.* 23, 320–330. <https://doi.org/10.1029/RS023i003p00320>.
- Kil, H., Kwak, Y.S., Paxton, L.J., Meier, R.R., Zhang, Y., 2011. O and N<sub>2</sub> disturbances in the F region during the 20 November 2003 storm seen from TIMED/GUVI. *J. Geophys. Res.* 116, A02314. <https://doi.org/10.1029/2010JA016227>.
- Kinrade, J., Mitchell, C.N., Smith, N.D., Ebihara, Y., Weatherwax, A.T., Bust, G.S., 2013. GPS phase scintillation associated with optical auroral emissions: first statistical results from the geographic South Pole. *J. Geophys. Res.* 118, 2490–2502. <https://doi.org/10.1002/jgra.50214>.
- Kintner, P.M., Ledvina, B.M., De Paula, E.R., 2007. GPS and ionospheric scintillations. *Space Weather*. 5(9).
- Klobuchar, J.A., 1987. Ionospheric time-delay algorithm for single-frequency GPS users. *IEEE Trans. Aerosp. Electron. Syst.* 3, 325–331.
- Li, G., Ning, B., Zhao, B., Liu, L., Wan, W., Ding, F., Xu, J.S., Liu, J.Y., Yumoto, K., 2009. Characterizing the November 2004 storm-time middle latitude plasma bubble event in Southeast Asia using multi-instrument observations. *J. Geophys. Res.* 114, A07304. <https://doi.org/10.1029/2009JA014057>.
- Loh, R., Wullschleger, V., Elrod, B., Lage, M., Haas, F., 1995. The U.S. Wide-Area Augmentation System (WAAS). *Navigation* 42, 435–465. <https://doi.org/10.1002/j.2161-4296.1995.tb01900.x>.
- Loucks, D., Palo, S., Pilinski, M., Crowley, G., Azeem, I., Hampton, D., 2017. High-latitude GPS phase scintillation from E region electron density gradients during the 20–21 December 2015 geomagnetic storm. *J. Geophys. Res.* 122. <https://doi.org/10.1002/2016JA023839>.
- MacDougall, J.W., 1990. The polar-cap scintillation zone. *J. Geomag. Geoelectr.* 42, 777–788.
- Mannucci, A.J., Tsurutani, B.T., Iijima, B.A., Komjathy, A., Saito, A., Gonzalez, W.D., Guarnieri, F.L., Kozyra, J.U., Skoug, R., 2005. Dayside global ionospheric response to the major interplanetary events of October 29–30, 2003 “Halloween Storms” *Geophys. Res. Lett.* 32, L12S02. <https://doi.org/10.1029/2004GL021467>.
- Mannucci, A.J., Tsurutani, B.T., Abdu, M.A., Gonzalez, W.D., Komjathy, A., Echer, E., Iijima, B.A., Crowley, G., Anderson, D., 2008. Superposed epoch analysis of the dayside ionospheric response to four intense geomagnetic storms. *J. Geophys. Res.* 113, A00A02. <https://doi.org/10.1029/2007JA012732>.
- Mannucci, A.J., Tsurutani, B.T., Kelley, M.C., Iijima, B.A., Komjathy, A., 2009. Local time dependence of the prompt ionospheric response for the 7, 9, and 10 November 2004 superstorms. *J. Geophys. Res.* 114, A10308. <https://doi.org/10.1029/2009JA014043>.
- Mannucci, A.J., Crowley, G., Tsurutani, B.T., Verkhoglyadova, O.P., Komjathy, A., Stephens, P., 2014. Interplanetary magnetic field  $B_Y$  control of prompt total electron content increases during superstorms. *J. Atmos. Sol. Terr. Phys.* 115. <https://doi.org/10.1016/j.jastp.2014.01.001>.
- Meggs, R.W., Mitchell, C.N., Smith, A.M., 2006. An investigation into the relationship between ionospheric scintillation and loss of lock in GNSS receivers, in *Characterising the Ionosphere*, N. Atlantic Treaty Organization, Res. and Technol. Organ., Neuilly sur-Seine, France, pp. 5-1–5-10.

- Meier, R.R., Crowley, G., Strickland, D.J., Christensen, A.B., Paxton, L.J., Morrison, D., 2005. First look at the November 20, 2003 super storm with TIMED/GUVI. *J. Geophys. Res.* 110, A09S41. <https://doi.org/10.1029/2004JA010990>.
- Misra, P., Enge, P., 2011. *Global Positioning System: Signals, Measurements and Performance: Revised*, second ed. Ganga-Jamuna Press, Massachusetts.
- Mitchell, C.N., Alfonsi, L., De Franceschi, G., Lester, M., Romano, V., Wernik, A.W., 2005. GPS TEC and scintillation measurements from the polar ionosphere during the October 2003 storm. *Geophys. Res. Lett.* 32, L12S03. <https://doi.org/10.1029/2004GL021644>.
- Nava, B., Rodríguez-Zuluaga, J., Alazo-Cuartas, K., Kashcheyev, A., Migoya-Orue, Y., Radicella, S., Amory-Mazaudier, C., Fleury, R., 2016. Middle- and low-latitude ionosphere response to 2015 St. Patrick's Day geomagnetic storm. *J. Geophys. Res.* 121, 3421–3438. <https://doi.org/10.1002/2015JA022229>.
- Nayak, C., Tsai, L.C., Su, S.Y., Galkin, I.A., Caton, R.G., Groves, K.M., 2017. Suppression of ionospheric scintillation during St. Patrick's Day geomagnetic super storm as observed over the anomaly crest region station Pingtung, Taiwan: a case study. *Adv. Space Res.* 60 (2), 396–405. <https://doi.org/10.1016/j.asr.2016.11.036>.
- Ngwira, C.M., Pulkkinen, A., Wilder, F.D., Crowley, G., 2013. Extended study of extreme geoelectric field event scenarios for geomagnetically induced current applications. *Space Weather* 11, 121–131. <https://doi.org/10.1002/swe.20021>.
- Nishioka, M., Tsugawa, T., Kubota, M., Ishii, M., 2013. Concentric waves and short-period oscillations observed in the ionosphere after the 2013 Moore EF5 tornado. *Geophys. Res. Lett.* 40, 5581–5586. <https://doi.org/10.1002/2013GL057963>.
- O'Hanlon, B.W., Psiaki, M.L., Powell, S., Bhatti, J.A., Humphreys, T.E., Crowley, G., Bust, G.S., 2011. CASES: a smart, compact GPS software receiver for space weather monitoring. In: *Proceedings of the 24th International Technical Meeting of the Satellite Division of the Institute of Navigation*, Portland, OR, pp. 2745–2753.
- Obama, B., 2016. Executive order—coordinating efforts to prepare the nation for space weather events. Available at <https://obamawhitehouse.archives.gov/the-press-office/2016/10/13/executive-order-coordinating-efforts-prepare-nation-space-weather-events>.
- Pi, X., Iijima, B.A., Lu, W., 2017. Effects of ionospheric scintillation on GNSS-based positioning. *NAVIGATION: J. Inst. Navigation* 64 (1), 3–22.
- Prikryl, P., Jayachandran, P.T., Mushini, S.C., Pokhotelov, D., MacDougall, J.W., Donovan, E., Spanswick, E., St. Maurice, J.-P., 2010. GPS TEC, scintillation and cycle slips observed at high latitudes during solar minimum. *Ann. Geophys.* 28, 1307–1316. <https://doi.org/10.5194/angeo-28-1307-2010>.
- Prikryl, P., Jayachandran, P.T., Mushini, S.C., Chadwick, R., 2011. Climatology of GPS phase scintillation and HF radar backscatter for the high-latitude ionosphere under solar minimum conditions. *Ann. Geophys.* 29, 377–392. <https://doi.org/10.5194/angeo-29-377-2011>.
- Prikryl, P., Zhang, Y., Ebihara, Y., Ghoddousi-Fard, R., Jayachandran, P.T., Kinrade, J., Mitchell, C.N., Weatherwax, A.T., Bust, G., Cilliers, P.J., Spogli, L., Alfonsi, L., De Franceschi, G., Romano, V., Ning, B., Li, G., Jarvis, M.J., Danskin, D.W., Spanswick, E., Donovan, E., Terkildsen, M., 2013a. An inter-hemispheric comparison of GPS phase scintillation with auroral emission observed at South Pole and from DMSP satellite. *Special Issue Annals Geophys.* 56 (2), R0216. <https://doi.org/10.4401/ag-6227>.
- Prikryl, P., Ghoddousi-Fard, R., Kunduri, B.S.R., Thomas, E.G., Coster, A.J., Jayachandran, P.T., Spanswick, E., Danskin, D.W., 2013b. GPS phase scintillation and proxy index at high latitudes during a moderate geomagnetic storm. *Ann. Geophys.* 31, 805–816. <https://doi.org/10.5194/angeo-31-805-2013>.
- Prikryl, P., et al., 2016. GPS phase scintillation at high latitudes during the geomagnetic storm of 17–18 March 2015. *J. Geophys. Res.* 121, 10448–10465. <https://doi.org/10.1002/2016JA023171>.
- Rama Rao, P.V.S., Gopi Krishna, S., Vara Prasad, J., Prasad, S.N.V.S., Prasad, D.S.V.V.D., Niranjan, K., 2009. Geomagnetic storm effects on GPS based navigation. *Ann. Geophys.* 27, 2101–2110.
- Ramsingh, S., Sripathi, S., Sreekumar, S., Banola, K., Emperumal, P., Tiwari, B.S., 2015. Kumar (2015), Low-latitude ionosphere response to super geomagnetic storm of 17/18 March 2015: results from a chain of ground-based observations over Indian sector. *J. Geophys. Res.* <https://doi.org/10.1002/2015JA021509>.

- Rao, N.V., Madhu, T., Kishore, K.L., 2010. Geomagnetic storm effects on GPS aided navigation over low latitude South Indian region. *Int. J. Comp. Sci. Network Sec.* 10(3). [http://paper.ijcsns.org/07\\_book/201003/20100306.pdf](http://paper.ijcsns.org/07_book/201003/20100306.pdf).
- Skone, S., Kundsen, K., deJong, M., 2001. Limitation in GPS receiver tracking performance under ionospheric scintillation conditions. *Phys. Chem. Earth* 26, 613–621. [https://doi.org/10.1016/S1464-1895\(01\)00110-7](https://doi.org/10.1016/S1464-1895(01)00110-7).
- Sparks, L., Blanch, J., Pandya, N., 2011a. Estimating ionospheric delay using kriging: 1. Methodology. *Radio Sci.* 46 (6). <https://doi.org/10.1029/2011RS004667>. 41–13.
- Sparks, L., Blanch, J., Pandya, N., 2011b. Estimating ionospheric delay using kriging: 2. Impact on satellite-based augmentation system availability. *Rad. Sci.* 46 (6). <https://doi.org/10.1029/2011RS004781>. 89–10.
- Spilker, J., 1978. GPS signal structure and performance characteristics. *J. Inst. Navigation* 25, 121–146.
- Spogli, L., Alfonsi, L., De Franceschi, G., Romano, V., Aquino, M.H.O., Dodson, A., 2009. Climatology of GPS ionospheric scintillations over high and mid-latitude European regions. *Ann. Geophys.* 27 (9), 3429–3437. <https://doi.org/10.5194/angeo-27-3429-2009>.
- Spogli, L., et al., 2016. Formation of ionospheric irregularities over Southeast Asia during the 2015 St. Patrick's Day storm. *J. Geophys. Res.* 121, 12211–12233. <https://doi.org/10.1002/2016JA023222>.
- Sreeja, V., Aquino, M., Elmas, Z.G., Forte, B., 2012. Correlation analysis between ionospheric scintillation levels and receiver tracking performance. *Space Weather.* 10, (6). S06005.
- Steenburgh, R.A., Smithro, C.G., Groves, K.M., 2008. Ionospheric scintillation effects on single frequency GPS. *Space Weather* 6, S04D02. <https://doi.org/10.1029/2007SW000340>.
- Tsugawa, T., Saito, A., Otsuka, Y., Nishioka, M., Maruyama, T., Kato, H., Nagatsuma, T., Murata, K.T., 2011. Ionospheric disturbances detected by GPS total electron content observation after the 2011 off the Pacific coast of Tohoku Earthquake. *Earth Planets Space* 63, 875–879.
- Tsurutani, B.T., Gonzalez, W.D., Lakhina, G.S., Alex, S., 2003. The extreme magnetic storm of 1–2 September 1859. *J. Geophys. Res.* 108 (A7), 1268. <https://doi.org/10.1029/2002ja009504>.
- Tulasi Ram, S., Rama Rao, P.V.S., Prasad, D.S.V.V.D., Niranjana, K., Gopi Krishna, S., Sridharan, R., Ravindran, Sudha, 2008. Local time dependent response of postsunset ESF during geomagnetic storms. *J. Geophys. Res.* 113. <https://doi.org/10.1029/2007JA01292>.
- Tulasi Ram, S., Yokoyama, T., Otsuka, Y., Shiokawa, K., Sripathi, S., Veenadhari, B., Heelis, R., Ajith, K.K., Gowtam, V.S., Gurubaran, S., et al., 2016. Duskside enhancement of equatorial zonal electric field response to convection electric fields during the St. Patrick's Day storm on 17 March 2015. *J. Geophys. Res.* 121, 538–548. <https://doi.org/10.1002/2015JA021932>.
- Vadas, S.L., Crowley, G., 2010. Sources of the traveling ionospheric disturbances observed by the ionospheric TIDDBIT sounder near Wallops Island on 30 October 2007. *J. Geophys. Res.* 115, A07324. <https://doi.org/10.1029/2009JA015053>.
- Vadas, S.L., Crowley, G., 2017. Neutral wind and density perturbations in the thermosphere created by gravity waves observed by the TIDDBIT sounder. *J. Geophys. Res.* 122, 6652–6678. <https://doi.org/10.1002/2016JA023828>.
- Van Dierendonck, A.J., 1999. Eye on the ionosphere: measuring ionospheric scintillation events from GPS signals. *GPS Solutions* 2 (4), 60–63.
- Ware, R., Exner, M., Feng, D., Gorbunov, M., Hardy, K., Herman, B., Kuo, H., Meehan, T., Melbourne, W., Rocken, C., Schreiner, W., Sokolovskiy, S., Solheim, F., Zou, X., Anthes, R., Businger, S., Trenberth, K., 1996. GPS sounding the atmosphere from low Earth orbit, preliminary results. *Bull. Am. Meteorol. Soc.* 77, 5–18.
- Wu, C.C., Liou, K., Lepping, R.P., Hutting, L., Plunkett, S., Howard, R.A., Socker, D., 2016. The first super geomagnetic storm of solar cycle 24: “The St. Patrick's day event (17 March 2015)”. *Earth Planets Space* 68, 151. <https://doi.org/10.1186/s40623-016-0525-y>.
- Zhang, S.-R., Zhang, Y., Wang, W., Verkhoglyadova, O.P., 2017. Geospace system responses to the St. Patrick's Day storms in 2013 and 2015. *J. Geophys. Res.* 122. <https://doi.org/10.1002/2017JA024232>.

## **FURTHER READING**

Trimble—GPS Tutorial—Error Correction, from [http://www.trimble.com/gps\\_tutorial/howgps-error2.aspx](http://www.trimble.com/gps_tutorial/howgps-error2.aspx)  
(Accessed July 2017).